communications engineering

A Nature Portfolio journal

Article

https://doi.org/10.1038/s44172-025-00574-4

Interaction-based rapid heuristic optimization of exoskeleton assistance during walking

Check for updates

Jianyu Chen[1,2,3], Weihao Yin[1,2,4], Jianquan Ding[1,2,4], Jiaqi Han[1,2,4], Lihai Zhang[5,6], Jianda Han[1,2,4] & Juanjuan Zhang[1,2,4]

Using human responses to optimize and thus personalize assistance enhances exoskeleton performance during locomotion. Current approaches lack efficiency, comfort, rapid deployability, and computation and actuation simplicity. Here we present a method that optimizes assistance within 2 min, 16 times faster than the state-of-the-art, by effectively imitating human joint moment while ensuring stability. Optimization of a unilateral ankle exoskeleton with off-board actuation produced gentler assistance (78.2% torque) while reducing muscle activity by 36.8% and metabolic cost by 20.4% than no assistance, comparable to state-of-the-art. The method was easily and effectively deployed across new gait conditions, to bilateral devices, to knee joints and also outdoors. It largely avoided the problems of existing methods with instantaneously measurable feedback, a non-aggressive tuning process, a reasonable tuning direction, and a non-parametric assistance formulation. By significantly reducing pre-research, operational, user physiological and psychological costs, this method largely elevates the accessibility level of effective, personalized and continuously tuned exoskeletons in everyday scenarios.

Lower-limb exoskeletons are meant to enhance human locomotion for various groups[1–12]. Not many have succeeded[5,7,9,13–23], due to the high complexity, time-varying property, and inter-personal differences of human bodies[5,18,24–29]. Among them, state-of-the-art exoskeleton planning methods mainly fall into two categories: instantaneous neural-network-based ones[21,22,30], and adaptive personalization-based ones[5,17]. The latter, by feeding human responses to optimize assistance using feasible algorithms[5,16,17,19,29,31,32], produces customized interactions and thus improves human mobility. It also prompts human safety, comfort, and computational simplicity. The strategy is effective since it closes a high-level control (i.e., assistance planning) loop of the human-exoskeleton coupled systems[5,29], in which the human body is the end-effector and the powered exoskeleton is the actuator as well as power transmitter (Fig. 1a).

Multiple works have demonstrated the effectiveness of this strategy[5,9,16,17,19,20,26,31,33–38]. A physiological measure, such as metabolic consumption, muscle activity and heart rate, usually served as the objective function, i.e., the feedback signal[5,9,16,17,34,39,40]. A rather long objective evaluation for each assistance condition was necessary to reduce the high noise of such signals by data processing. For example, metabolic consumption was often evaluated with data of a 2-min period to accommodate the long stabilization time of respiratory readings[5,9,16,26]. Muscle activity through electromyography, which is easily disturbed[41], was usually measured for tens of seconds to 2 min in evaluation[34,39,42]. Psychological measures like user preference were noisier and more time-consuming as objectives[19]. A more recent work[17] managed to evaluate one condition within 30 s by indirectly signaling metabolism using motion data. However, humans, especially the gait-impaired ones, can only walk continuously and consistently for limited lengths of time. Therefore, only optimization algorithms that can survive high noise and small sample sizes will work. Covariance matrix adaptation-evolutionary strategy (CMA-ES) has been the state-of-the-art choice[5,9,17,20,26,29,35] due to its tolerance to sensor noise, local optima, human adaptation and large parameter dimensions[29,43].

Existing closed-loop adaptive assistance optimization approaches using CMA-ES, although effective, bear some major limitations, e.g., long optimization protocols, compromised user comfort, long pre-research time for new applications, and relatively high required computational power and actuation capacity. Long condition evaluation leads to lengthy optimization tests. Currently, a typical optimization process of 2–4 parameters for a

[1]College of Artificial Intelligence, Nankai University, Tianjin, PR China. [2]Institute of Robotics and Automatic Information System, Nankai University, Tianjin, PR China. [3]Hangzhou Zhiyuan Research Institute Co., Ltd, Zhejiang, PR China. [4]Academy for Advanced Interdisciplinary Studies, Nankai University, Tianjin, PR China. [5]National Clinical Research Center for Orthopedics, Sports Medicine, and Rehabilitation, Beijing, PR China. [6]School of Medicine, Nankai University, Tianjin, PR China. e-mail: juanjuanzhang@nankai.edu.cn

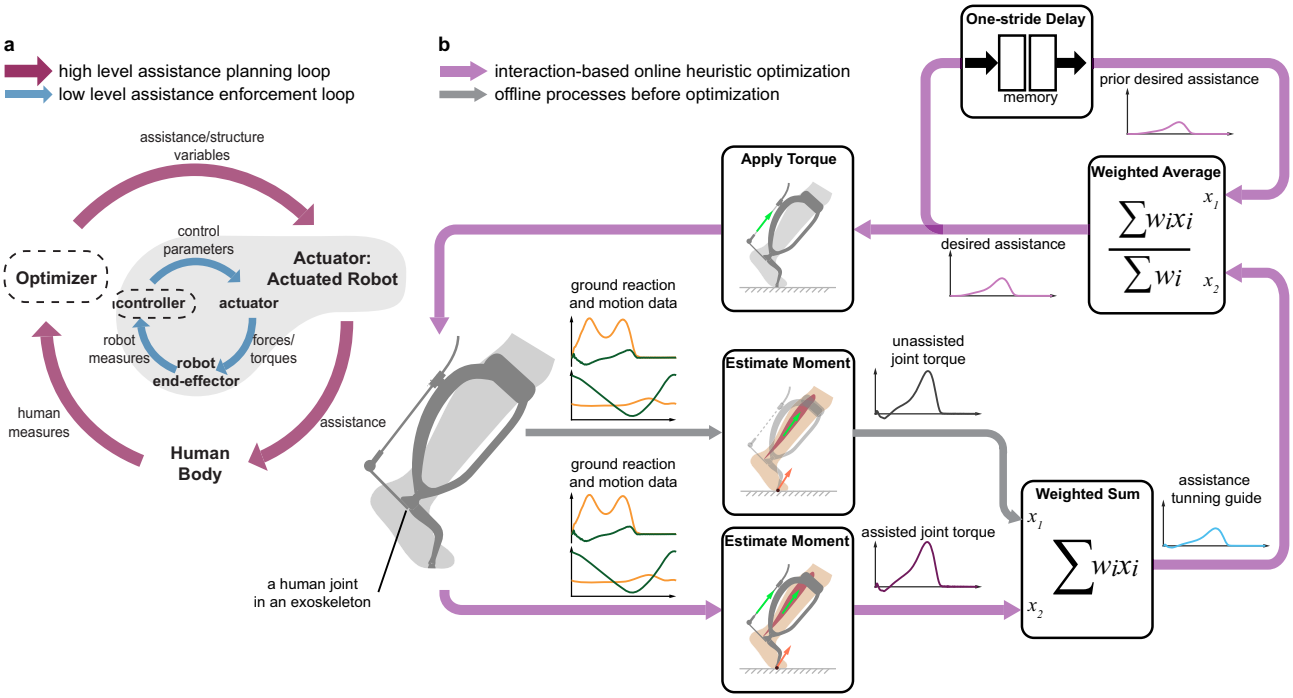

Fig. 1 | Interaction-based rapid heuristic optimization. a Feeding human measures to optimize assistance-related parameters in human-robot interactive systems closes a high level control (i.e., assistance planning) loop. **b** A rapid heuristic method to feed measured joint torques of human-exoskeleton coupled system to optimize desired assistance. Ground reactions and joint motions were measured to calculate assisted and unassisted joint torques. A weighted sum of real-time assisted joint torque and pre-measured unassisted one served as a guide, which directed the iterative tuning of the desired assistance.

1-degree-of-freedom exoskeleton takes tens of minutes[5,9,16,17,20,26,35,38]. Algorithm-based random sample generation means many never-experienced and unknown assistance conditions for users wearing the exoskeleton[43]. This suppresses the influences of measurement noises and local extrema on optimization performance. It forces a diverse exploration of assistance profiles and thus an intensive training. Both contribute to the success of CMA-ES in this application[5], but only provided that parameter search ranges are not overly constrained. This wide and random exploration incurs physical and psychological user discomfort, more required actuation capacity and relatively high computational power. Besides challenges for users, the strategy also poses ones for developers. CMA-ES tries to optimize values for a set of variables. Meanwhile, the exoskeleton assistance to be optimized is a one-stride-long continuous-time curve (e.g., torque). To overcome this format mismatch, one has to properly define a general assistance profile, parametrize it, and set initial values, ranges, as well as update step sizes for the parameters. These require careful pre-research on the characteristics of specific joints, gait conditions, user groups, and assisting exoskeletons.

In exoskeleton assistance planning, it is intuitive to imitate human biomechanics. Approaches that directly map instantaneous joint moment estimates or muscle activities to assistance torque[8,10,30,44] embody this straightforward principle. The efficacy of such strategies depends on an efficient and cooperative human–machine interaction. However, their intrinsic positive-feedback-loop nature places the burden of achieving this synergy entirely on the user's neuromuscular system. A user failure at reacting cooperatively and instantaneously may incur system instability and human danger. A recent study[45] introduced the Interaction Portrait metric to evaluate such interaction properties, underscoring the need for strategies that promote cooperative dynamics. For strategies based on human biomechanics, a proper closed-loop adaptive structure can potentially provide the necessary environment and constraints to foster a stable and effective exoskeleton-assisting-human interface.

Wrestling limitations of current exoskeleton assistance planning strategies, we have developed a rapid closed-loop optimization approach that tried to mimic human natural mechanics while partially replacing human efforts with exoskeleton assistance. It stride-wise tuned assistance torque towards a hybrid direction of two references: (1) the real-time combined joint torque produced by the human and exoskeleton (referred to as "assisted joint torque" hereinafter), and (2) a pre-measured baseline of the human joint torque recorded while the participant walked wearing the exoskeleton without assistance ("unassisted joint torque" or "human torque in zero-torque mode"). At any time, the desired assistance was set as the weighted average of two items: its prior value at the same time of the last stride period, which was made dominant to ensure a gentle tuning process; and a tuning guide defined by a weighted sum of the assisted and unassisted joint torques (Fig. 1b, Eq. (1) in "Methods").

The approach closed a high-level control loop by facilitating real-time continuous interactions between assistance and assisted joint torque. It realized a gradient descent optimization process[46] that minimized the combination of human torque, exoskeleton inputs and assistance-incurred biomechanical changes (Eq. (2), "Methods"). It ensured safe, stable and cooperative human-exoskeleton interactions through the closed-loop adaptive framework and appropriate constraints.

Instantaneous evaluation of the feedback signal, i.e., the assisted joint torque, significantly shortened the optimization process. Small stride-wise assistance changes and the rather natural tuning directions ensured user comfort and reduced the actuation capacity required. Non-parametric assistance formulation and direct association between assistance and assisted joint torque saved pre-research time on human biomechanics to construct and then parameterize assistance profiles when application scenarios changed. Besides, condition evaluation and assistance updation both required only a few basic arithmetic operations. Computation and actuation simplicity suggested easier outdoor applications.

Results

We tested the performance of the proposed method by optimizing the assistance of a unilateral single-degree-of-freedom plantarflexion ankle exoskeleton[47] during human walking (Fig. 2a, b). Experiments were conducted on a versatile emulator system[47] inspired by previous designs[5,48], which allowed effective assistance updation, precise realization[49] and easy switching

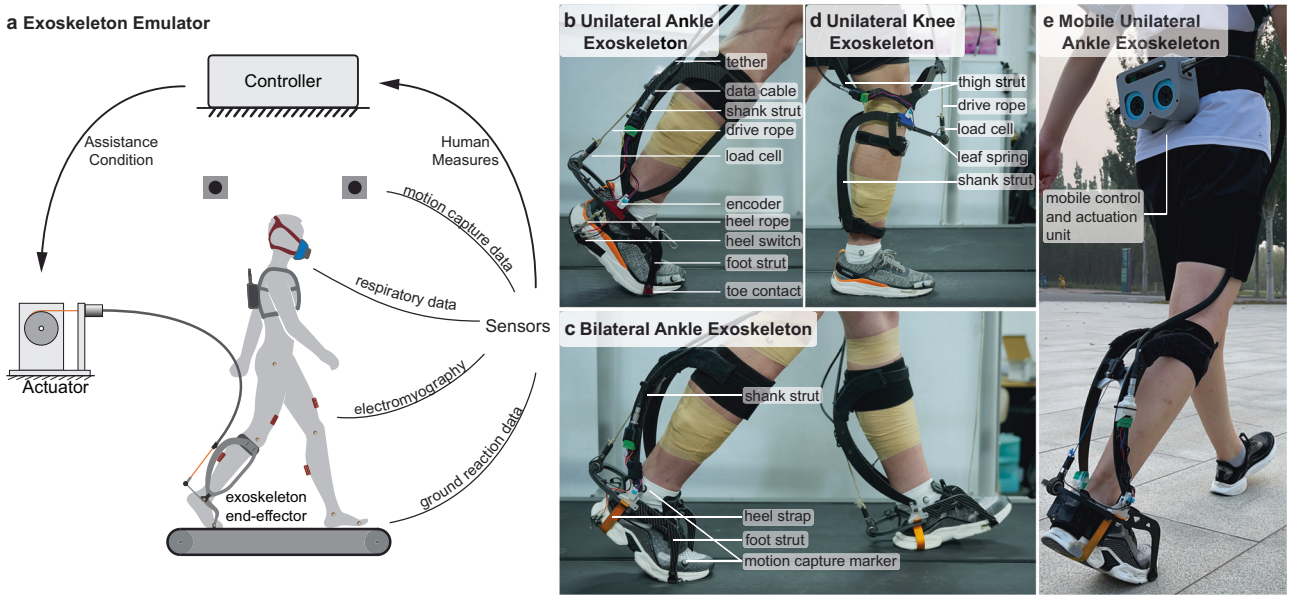

Fig. 2 | Exoskeleton testbeds. a The in-laboratory testbed composed of a powered exoskeleton, a high-speed controller, multiple sensors for human measures. **b** Photo of the unilateral ankle exoskeleton worn on the right foot used in main, generality and convergence studies. **c** Photo of the bilateral ankle exoskeleton worn on both feet in generality tests. **d** Photo of the unilateral knee exoskeleton worn on the right leg in generality tests. **e** Photo of the mobile unilateral ankle exoskeleton worn on the right foot for outdoor generality tests.

of exoskeleton end-effectors (Supplementary Fig. 1). This system was chosen to facilitate easy comparison with a previous study[5] directly minimizing human physiological measures with CMA-ES, which represents state-of-the-art assistance optimization performance. That study[5] not only used an emulator system that closely mirrored ours, with the same motor model and a similar end-effector design, but also reported both human metabolic and muscular benefits like ours. It thus served as the primary reference for optimization performance. Another key control study[17] demonstrated comparable energy benefit with shorter optimization processes, which represents state-of-the-art optimization efficiency and served as the benchmark for convergence speed. Every participant went through an assistance optimization process during walking and a double-reversal validation process. In updating the desired assistance torque during optimization, we set the weights of prior assistance torque ($1-\alpha$, Eq. (1)) and the tuning guide (α, Eq. (1)) to be 0.975 and 0.025, respectively. In forming the guide, assisted and unassisted joint torques were equally weighted in the range of [0.175, 0.25]. The optimization processes lasted for 2 min for all participants.

We optimized assistance of the unilateral ankle exoskeleton for 10 participants (P1–P10, Supplementary Table 1) while they walked on a treadmill at a moderate speed (1.25 m s^{-1}) in the main study. In validation, optimized assistance profiles were compared with zero-torque and normal-shoe mode in which the participants walked wearing their normal shoes without exoskeletons. Seven out of the ten participants also walked with a generic assistance achieved by averaging the optimized assistance profiles of all participants in literature[5]. The remaining three found it unbearable, which suggested that the comparison between the optimized and generic conditions using data of the seven participants favored the latter.

Improvements in human muscle economy

Human muscle economy was significantly improved for all participants in validation (Fig. 3a, c; individual data are in Supplementary Fig. 5). Optimized assistance reduced the activities of soleus muscle on the assisted side by 36.8 ± 13.3% (mean ± standard deviation, ranging from 22.0 to 57.1%) compared to zero-torque mode (Fig. 3a, $n = 10$, t test, Holm–Bonferroni correction, adjusted $P = 1.1E-4$), by 36.6 ± 13.6% (ranging from 21.0 to 61.5%) compared to normal-shoe mode (Fig. 3a, $n = 10$, t test, adjusted $P = 1.1E-4$), and by 15.0 ± 7.0% (ranging from 7.6 to 29.6%) compared to the generic condition (Fig. 3c, $n = 7$, t test, adjusted $P = 3.0E-3$). In comparison, with a state-of-the-art approach using CMA-ES to directly minimize soleus activity for a similar exoskeleton, a 32-min optimization process[17] led to a decrease in soleus activity by 41%[5] (Fig. 3e, $n = 1$).

Improvements in human metabolic economy

Validation of the main study also demonstrated significant improvements in human metabolic economy through rapid optimization (Fig. 3b, d; individual data in Supplementary Fig. 6). Optimized assistance reduced participants' net walking metabolic costs by 20.4 ± 11.4% (ranging from 7.8 to 39.1%) compared to zero-torque mode (Fig. 3b, $n = 10$, t test, adjusted $P = 3.0E-3$), by 19.7 ± 10.3% (ranging from 5.9 to 38.1%) compared to the normal-shoe mode (Fig. 3b, $n = 10$, t test, adjusted $P = 3.0E-3$), and by 13.7 ± 9.8% (ranging from 2.9 to 30.5%) compared to the generic condition (Fig. 3d, $n = 7$, t test, adjusted $P = .8E-2$). In comparison, with a state-of-the-art approach using CMA-ES to directly minimize metabolic costs[5], 32-min optimization processes[17] produced net metabolic cost reduction of 24.2% (Fig. 3f, $n = 11$).

Improvements in human joint mechanics

Human joint mechanics were modified by the optimized assistance in validation for all participants (Fig. 4 and Supplementary Figs. 7–10). Combined human-exoskeleton joint torque with optimized assistance shifted a little from the unassisted torque along gait cycle (Fig. 4a), but rose obviously on the ankle angle axis and produced increased mechanical work input to human body (Fig. 4b). This aligned with the observation that the assisted ankle power curve shifted earlier in mid-stance, causing a decrease in negative power and an increase in positive power (Fig. 4c). With optimized assistance, average stride-wise positive ankle work increased by 25.4 ± 15.7% ($n = 10$, t test, adjusted $P = 3.0E-3$) compared to zero-torque mode, ranging from −2.1 to 47.0%, and by 36.0 ± 25.6% ($n = 10$, t test, adjusted $P = 3.0E-3$) compared to normal-shoe mode, ranging from 5.9 to 78.3% (Fig. 4d).

Customization of assistance torque profiles

The customization functionality of the method was demonstrated by the individualized optimized assistance profiles (peaked at 0.602 ± 0.088 Nm kg^{-1}, $n = 10$, Fig. 3h, Supplementary Fig. 7), each close to its guide at steady state (Fig. 4a), and lower than state-of-the-art[5] (peaked at 0.770 ± 0.086 Nm kg^{-1}; $n = 11$, two-tailed unpaired t test, adjusted $P = 8.3E-4$). Consequentially, work loops (Supplementary Fig. 8), joint power

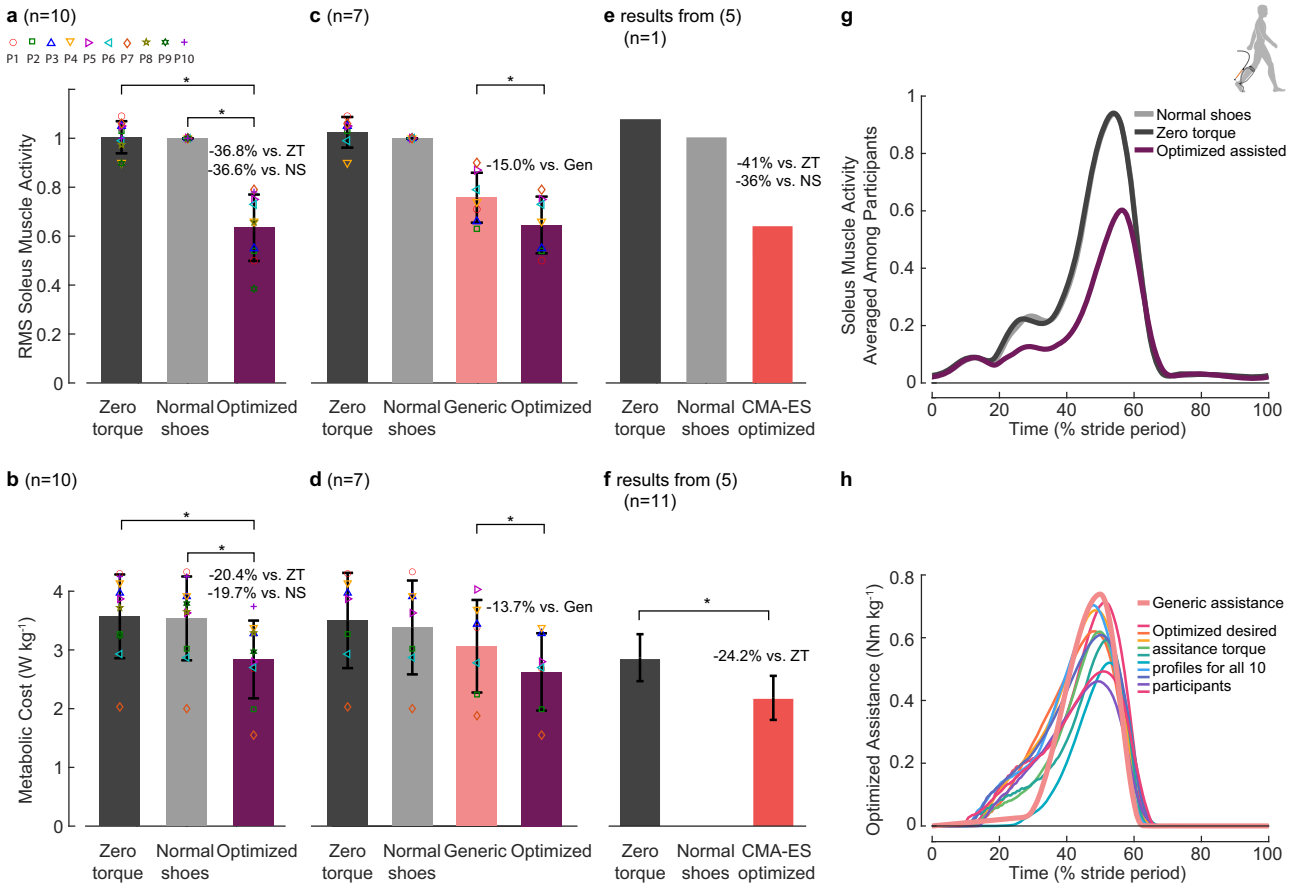

Fig. 3 | Physiological and customization results of the main experimental study. **a** Root-mean-squared soleus muscle activity in zero-torque, normal-shoe and optimized conditions of walking measured in validation trials, normalized to that of normal-shoe condition. Optimized assistance resulted in large reductions compared to the zero-torque and normal-shoe conditions ($n = 10$). Variability is due to differences between participants. Bars are means, error bars are standard deviations, individual markers denote data from different participants, and asterisks denote statistical significance ($P < 0.05$). **b** Metabolic consumption during validation. Optimized assistance resulted in reductions compared to the zero-torque and normal-shoe condition ($n = 10$). **c** Seven out of ten participants also walked with a generic assistance condition achieved by averaging the optimized profiles of state-of-the-art[5] using Covariance Matrix Adaptation-Evolutionary Strategies (CMA-ES) to directly minimize metabolic costs. Optimized assistance saw 15% ($n = 7$) less soleus activity compared to the generic condition. **d** Optimized assistance saved 13.7% net metabolic costs compared to the generic condition ($n = 7$). **e** Root-mean-squared soleus muscle activity in different conditions in ref. 5 using CMA-ES to directly optimize soleus activity. **f** Metabolic costs in different conditions in ref. 5 using CMA-ES to directly minimize energy consumption. **g** Average soleus activities along the strides for different conditions. Optimized assistance reduced muscle activities mainly during early plantarflexion. **h** Optimized ankle exoskeleton torque profiles for each participant and the generic assistance profile. Lines are desired torque trajectories normalized to the gait cycle and body mass. Optimized assistance varied widely among participants, all of which had peak torque lower than that of the generic condition.

(Supplementary Fig. 9), corresponding improvements in human muscle (Supplementary Fig. 5), metabolic (Supplementary Fig. 6) and mechanical economies (Supplementary Fig. 10) all varied among participants.

Convergence of optimization and effects of the learning rate

We tested the convergence of the method and effects of learning rate, i.e., the weight of tuning guide in assistance updation (α in Eq. (1)), by optimizing the assistance from multiple initial locations and with multiple learning rates, separately, for one participant (P1), with the same emulator as the main study. With different learning rates, optimization converged to a similar area but with different rise time lengths (Fig. 5a). Regardless of its starting position, the desired assistance converged to locations in close vicinity to one another (Fig. 5b).

Generality under different gaits, devices and joints, and outdoor environment

We tested the generality of the proposed approach in the lab under different gait conditions, assisting devices and assisted joints, and outdoors, with a series of single-subject (P1) studies. In all cases, optimization produced proper assistance profiles (Fig. 6a–d) that improved human economy (Fig. 6e–h). When assisted by the same unilateral ankle exoskeleton as main study[47] (Fig. 2b), optimized assistance reduced soleus muscle activities and metabolic costs of the participant (Fig. 6i, m) walking at a slow speed (1.0 m s^{-1}; 47.6% and 33.6% respectively versus normal-shoe), walking at a medium speed (1.25 m s^{-1}; 42.2% and 25.4%), walking at a fast speed (1.5 m s^{-1}; 48.1 and 18.3%), walking while loaded (vest weighting 20% of body mass; 1.25 m s^{-1}; 32.7% and 35.5%), walking uphill (10° incline; 1.25 m s^{-1}; 26.3% and 16.9%) and running (2.5 m s^{-1}; 47.8% and 19.7%). When assisted by a bilateral plantarflexion ankle exoskeleton[50] (Fig. 2c), optimized assistance reduced soleus muscle activity and metabolic cost walking at a medium speed (1.25 m s^{-1}) by 41.1% and 32.9% respectively, compared to zero-torque mode, and 34.8% and 30.9% compared to normal-shoe mode (Fig. 6j, n). We also optimized the assistance of a single-degree-of-freedom knee extension exoskeleton (Fig. 2d and Supplementary Fig. 3) while the participant walked uphill (5°) on the treadmill at a medium speed (1.25 m s^{-1}). Rectus femoris activity was reduced by 48.6% and 49.1% with optimized assistance compared to zero-torque and normal-shoe modes (Fig. 6k). Corresponding metabolic cost reductions were 15.5% and 11.5% (Fig. 6o). In an outdoor test of the method on a mobile unilateral plantarflexion ankle exoskeleton (Fig. 2e and Supplementary Fig. 2), optimized

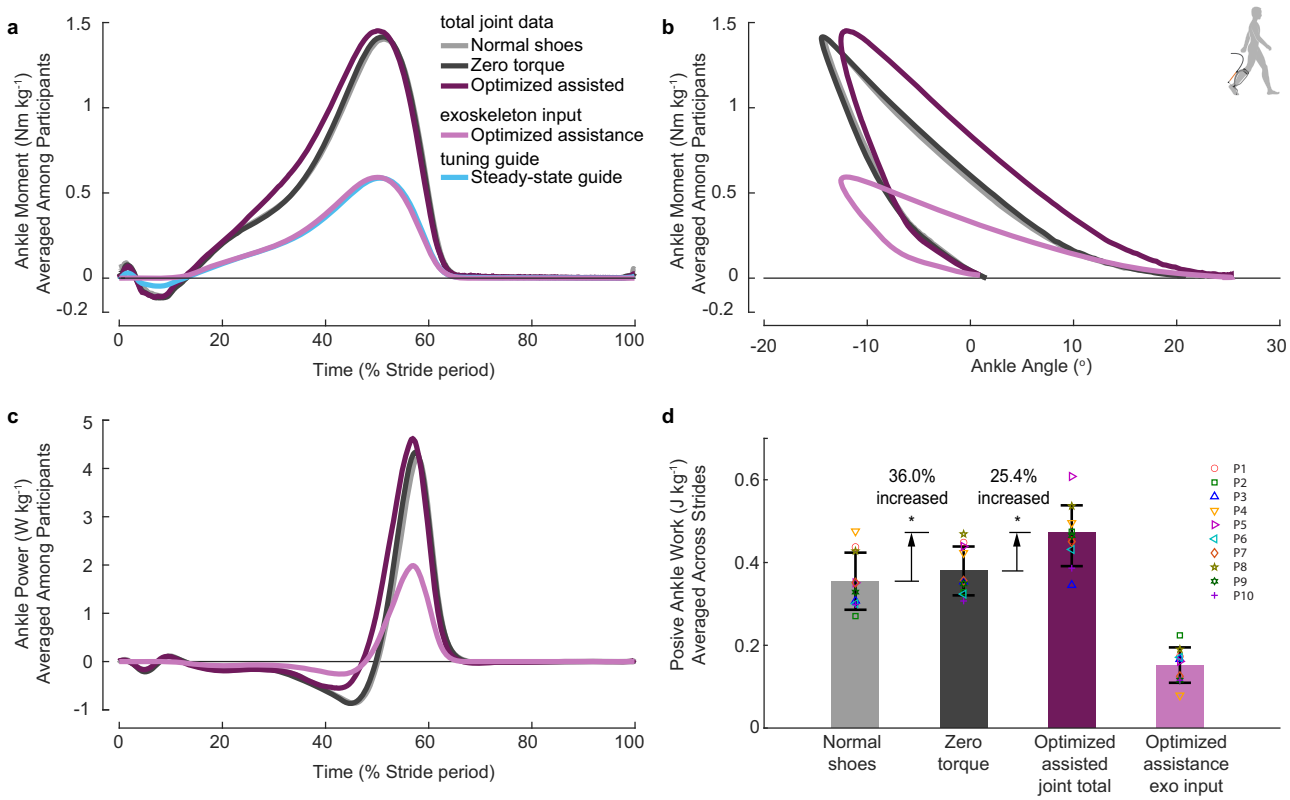

Fig. 4 | Mechanical results of the main experimental study. a Total ankle moments of different conditions (optimized, zero-torque and normal-shoe) and optimized assistance torque measured in validation trials, in comparison with the steady-state guide profile in optimization trials, all averaged across 10 participants (So is in (**b**, **c**)). **b** Average torque versus angle curves. **c** Ankle power of each condition and input mechanical power of the optimized assistance measured in validation trials averaged among participants. **d** Average stride-wise positive ankle mechanical work ($n = 10$) for different conditions and exoskeleton input work for optimized assisted condition in validation. Individual markers denote data from different participants.

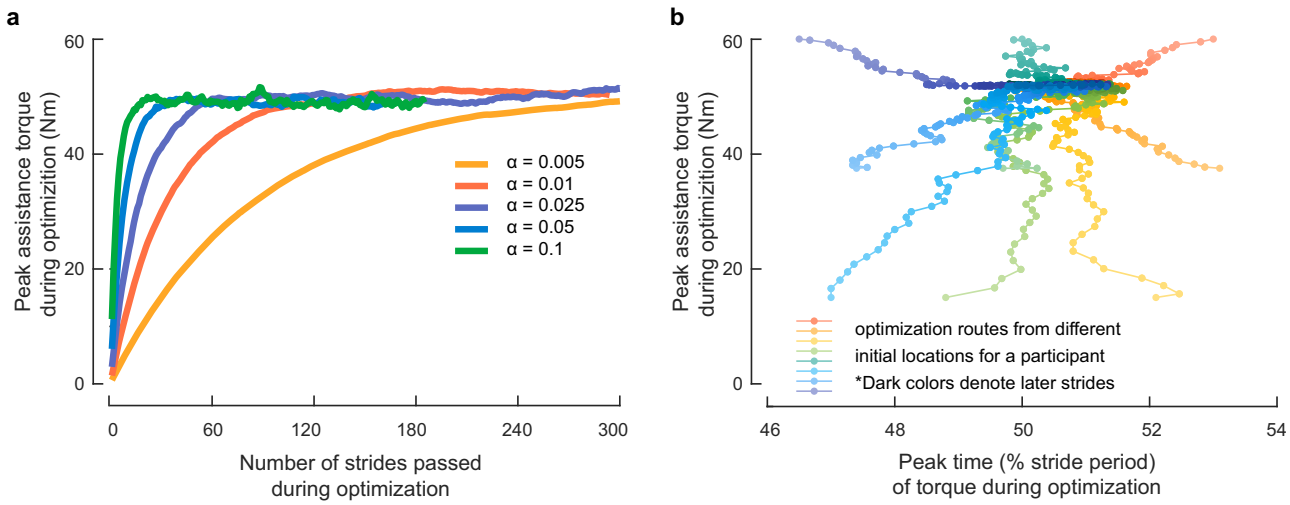

Fig. 5 | Experimental results of single-participant studies to test assistance optimization convergence with different learning rates and initial values. a Stride-wise peak desired assistance torque during optimization with five different learning rates, i.e., weight of the tuning guide. **b** Routes of the position of peak desired assistance torque and the time it happens within the stride, starting from different initial values. Higher color saturation denotes later strides in optimization.

assistance reduced soleus muscle activity of walking at user-preferred speed by 36.9% compared to zero-torque mode (Fig. 6l).

Comparison with assistance proportional to real-time assisted joint torque

We evaluated the performance of the strategy that applied a portion of real-time joint torque, with four different proportional gains (K_f = [0.2, 0.3, 0.4, 0.5]), on the unilateral ankle exoskeleton (Fig. 2b) to indirectly compare them with the proposed method. Higher gains were associated with reduced voluntarily reported tolerability. Four out of six participants (Supplementary Table 3) recruited could walk with more than half of the conditions and had data recorded, and only three went through all four gains. Participant feedback consistently characterized the proportional real-time joint moment as "difficult to control",

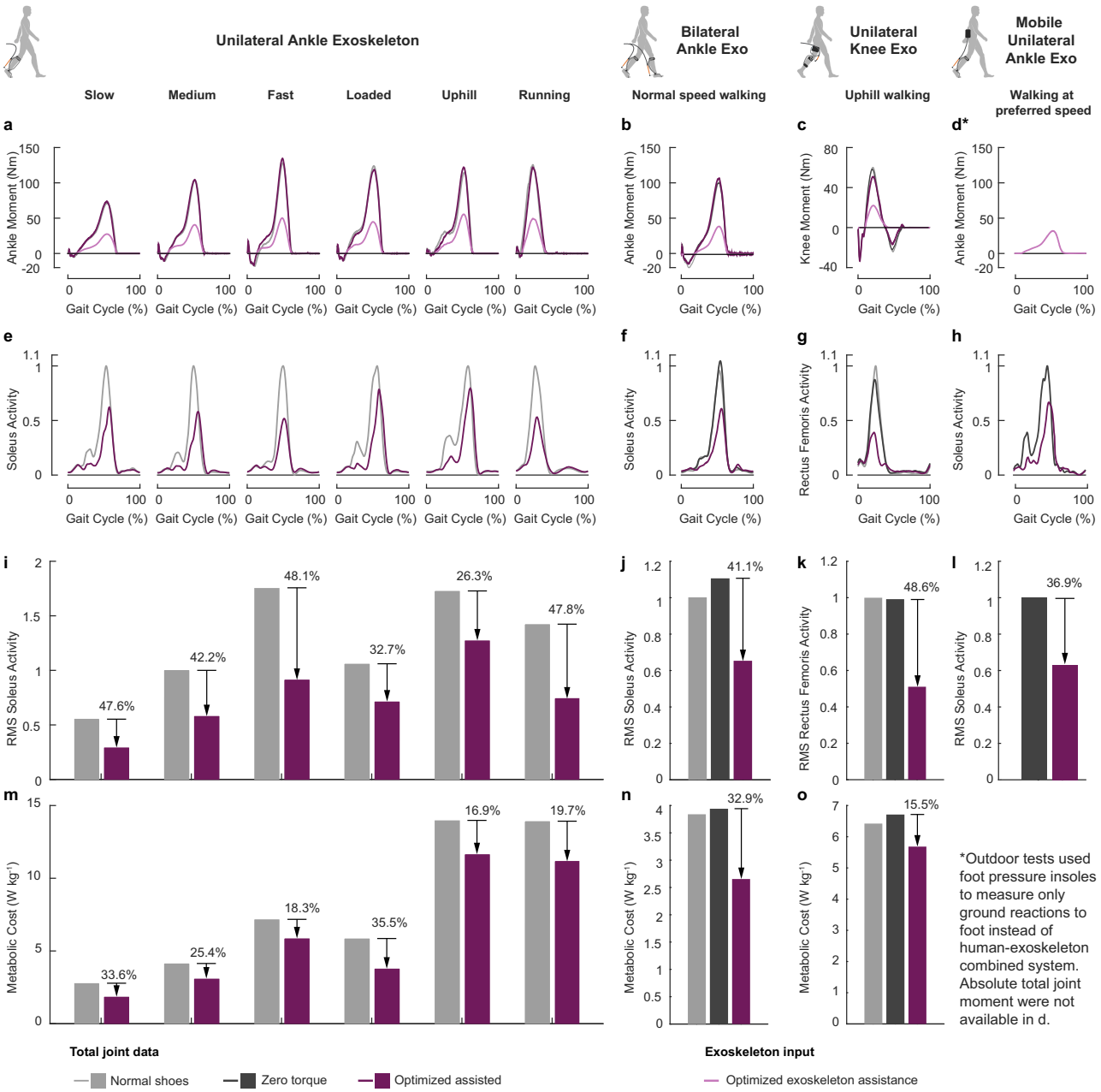

Fig. 6 | Experimental results of single-participant generality tests. a–d Optimized desired assistance torque and average joint moments of different assistance modes (normal-shoe and optimized assisted for all three in-lab exoskeleton systems; zero-torque modes also for the bilateral ankle and the unilateral knee exoskeleton systems; none for mobile system due to different way of measuring ground reaction) along the gait cycle under different gait conditions (speed, terrain, loading, running), assisting devices (unilateral, bilateral, mobile, knee) and assisted joints (ankle, knee). **e–h** Average local muscle activities of different modes and conditions along the gait cycle. **i–l** Root-mean-squared local muscle activity of different assistance modes and conditions. Muscle economy was significantly improved for all conditions. **m–o** Metabolic costs of different conditions. Metabolic economy was substantially improved for all conditions.

whereas the heuristic optimization was generally perceived as "rather comfortable".

The reductions in soleus activity of the four conditions from zero-torque condition, were 8.7 ± 8.5% (K_f = 0.2, n = 4, paired t test, Holm-adjusted P = 0.67), 12.9 ± 8.9% (K_f = 0.3, n = 4, adjusted P = 0.38), 28.2 ± 11.3% (K_f = 0.4, n = 4, adjusted P = 0.12) and 35.8 ± 9.3% (K_f = 0.5, n = 3, adjusted P = 0.15) respectively (Supplementary Fig. 12). Stride-wise positive ankle work increased by − 1.9 ± 10.0% (K_f = 0.2, n = 4, paired t test, adjusted P = 1), 2.6 ± 15.9% (K_f = 0.3, n = 4, paired t test, adjusted P = 0.77), 5.0 ± 24.8% (K_f = 0.4, n = 4, paired t test, adjusted P = 1) and 16.9 ± 26.8% (K_f = 0.5, n = 3, paired t test, adjusted P = 1).

Comparison with assistance proportional to unassisted joint torque

We also compared the proposed method to another generic assistance (Gen2), which asserted assistance proportional to the baseline joint torque during zero-torque mode (Supplementary Fig. 13) at low torque, for three participants (Supplementary Table 4). Optimized condition demonstrated muscle activity reduction of 25.1 ± 13.6% (n = 3, 10.7% to 37.6%, adjusted P = 0.85), and 4.5 ± 1.4% (n = 3, 3.0% to 5.8%, adjusted P = 0.70), from zero-torque and Gen2 conditions, respectively. Average peak asserted torques of Gen2 and optimized conditions were 0.391 and 0.410 Nm kg^{-1} (Supplementary Fig. 13a). Two participants (P14, P2) voluntarily reported Gen2

condition to be more intolerable than the optimized. The lack of statistically significance in muscle benefit was likely due to low tested assistance torque and small sample size.

Discussion

Different perspectives on the proposed method

The proposed rapid optimization method (Eq. (1)) can be interpreted through several foundational perspectives, whose interplay gave rise to its different functional properties and performance outcomes.

The simple update law (Eq. (1)) constitutes an iterative learning process with a forgetting factor (1-α), which progressively adjusts exoskeleton torque toward a dynamic guide. The guide comprised the downscaled time-invariant unassisted joint torque, which served as a nominal destination, and the downscaled time-varying assisted joint torque, which introduced adaptive deviations from the nominal curve.

The online tuning approximates a gradient descent optimization[46] that minimizes a cost function comprising human torque, exoskeleton assistance and exoskeleton-induced changes of total joint torques (Eq. (2), "Methods"), in which the last objective is prioritized. As human and exoskeleton torques constitute the assisted joint torque, this formulation encouraged the maintenance of natural joint biomechanics while efficiently offloading muscular effort with minimal exoskeleton input.

Furthermore, the tuning rule forms a positive feedback loop between the exoskeleton torque and the real-time assisted joint torque, with the positive gain (K_{dev}, Eq. (1)) set for the assisted torque in this study.

This is an exoskeleton optimization process that leverages human intrinsic motor optimization. The algorithm dynamically adjusts the assistance to track the assisted joint torque, which resulted from human adaptation to the exoskeleton's intervention. By creating a structured environment that facilitated human-machine cooperation, it ensures that the assisted torque adapt optimally and be a reliable tracking target.

Performance relative to state-of-the-art personalization-based methods

The proposed rapid heuristic method improved human economy efficiently and effectively with personalized exoskeleton assistance planning. Compared to the state-of-the-art approach using CMA-ES to directly minimize human economy[5,17], with 1/16 of the optimization duration[17], 21.8% smaller peak torque (0.602 vs. 0.770 Nm kg^{-1}) and for a similar unilateral ankle exoskeleton, the optimized assistance achieved comparable local muscle activity reduction ($n = 10$, $36.8 \pm 13.3\%$ vs. $n = 1$, 41%[5], two-tailed unpaired t test, adjusted $P = 0.77$) and comparable walking metabolic cost reduction ($n = 10$, 20.4% vs. $n = 11$, 24.2%[5], two-tailed unpaired t test, adjusted $P = 0.74$) from zero-torque mode. Meanwhile, its optimization process proved to be more comfortable and simpler in terms of computation and actuation. Its effectiveness has also been easily transferred to different gait conditions, devices and joints.

The short optimization process was the combined result of instantaneous feedback evaluation and fast optimization convergence. In optimizing the plantarflexion assistance of a similar unilateral exoskeleton, the rapid optimization here lasted 1/32 of the duration using CMA-ES to minimize metabolic consumption for a 4-parameter assistance[5], 1/24 of that for a 2-parameter one[34], and 1/16 of that to minimize motion changes[17]. Fast evaluation of real-time assisted torque was based on ground reaction and motion data, both of which were measured instantaneously with relatively low noises. Convergence speed was mostly related to learning rate (α in Eq. (1); Fig. 5a). We set it as 0.025 and the assistance took around (not exact, due to the presence of the time-varying assisted torque) 40 strides to rise to its steady-state value. We set an optimization length of about three times this rise period, 2 min. Within this time, assistance profiles starting from different values, under different gaits, for different devices and joints, all converge (Figs. 3, 4, 5b and 6).

The effectiveness of the proposed method in optimizing exoskeleton assistance was attributed to its nature as a closed-loop adaptive optimization strategy with appropriate objectives and constraints. The assisted joint torque, which comprised human and exoskeleton torques, served as a feedback signal and included human in high-level control loop. Besides, assistance tuning with this method was approximately equivalent to a gradient descent optimization. Therefore, it achieved both "closed-loop" and "optimization". However, the implementation of a human-in-the-loop optimization does not inherently guarantee user benefit. The feedback signal or objective function must be designed to correlate with physiologically meaningful human outcomes. Real-time assisted joint torque is the result of human optimal adaptation to gradually changing exoskeleton interventions. Consequently, using it as feedback meant a meaningful human-body-optimized tuning direction. On another note, the positive feedback loop between exoskeleton torque and assisted joint torque was purposely designed to encourage growth of exoskeleton torque, by exploiting the inherent diverging property of such loops, to produce meaningful assistance. In contrast, a negative feedback loop ($K_{dev} < 0$) would minimize the torque and cause the tuning process to fail. Crucially, the presence of the nominal guide (the assisted joint torque) constrained assistance divergence, ensuring system stability and preventing human injuries. On top of all these, user comfort throughout the optimization process prevented fight-or-flight responses and nurtured human-machine cooperation[51,52]. It represented an important factor why the feedback, i.e., assisted joint torque, was optimally adapted, and thus, such a short process turned out to be so effective.

The approach achieved user comfort during optimization by both minor stride-to-stride assistance changes and non-strange assistance profiles at all strides. The former was ensured by the choice of a non-aggressive assistance learning rate. With a 0.025 rate set in this study, and a maximumly [0.25 0.25] weight of assisted and unassisted joint torques in the guide, the stride-wise change on the assistance was less than 2 Nm for a 70 kg participant with 100 Nm peak unassisted joint torque. The non-strange real-time assistance, on the other hand, was the combined effect of a reasonable starting position, a rather natural tuning direction and a bounded final assistance. In all experiments except the one demonstrating algorithm convergence by different routes (Fig. 5b), we started the assistance from a series of zeros. The tuning direction and constraints were both governed by the guide comprising pre-defined portions of time-invariant unassisted joint torque and time-varying assisted joint torque. Both unassisted and assisted torque resulted from natural human adaptation: the former to exoskeleton's structure and mass, and the latter to active intervention, remaining closely around the unassisted. With small equal weight values ($0.175 \le K_{nom} = K_{dev} \le 0.25$) set for the guide, real-time assistances were modest in terms of both magnitude and profile.

The comfortable optimization produced comfortable optimized assistance through different optimization routes and learning rates (Figs. 4a and 5). The assistance peak torque was lower compared to literature[5]. Moreover, the resulting optimized assisted joint torque deviated relatively little from the unassisted one along the axis of tuning (i.e., time in stride for this study, Fig. 4a), while exerting significantly more mechanical power (Fig. 4b–d). This was attributed to the tuning algorithm, which partially minimized the difference between assisted and unassisted joint torques (Eq. (2)).

Moreover, the algorithm determined that the optimized assistance converged to the steady-state guides (Fig. 4a; Supplementary Fig. 7 and Supplementary Table 2) made of the downscaled optimized assisted and unassisted total joint torques ($K_{dev}\tau_{joint} + K_{nom}\tau^{ZT}_{joint}$). The close adjacency of these two torque profiles also positioned the final assistance around $K_{dev} + K_{nom}$ times the unassisted one. This outcome was deliberate, achieved through participant-selected guide gains (K_{nom}, K_{dev}), with the principal optimization results manifesting as deviations from the designed nominal profile ($(K_{dev} + K_{nom})\tau^{ZT}_{joint}$).

The rapid optimization greatly reduced muscle activities since the feedback that included human in the loop, i.e., the human portion of total assisted joint torque, was essentially produced by muscle forces. Therefore, comparable improvements in muscle economy were achieved with state-of-the-art using CMA-ES to directly minimize muscle activity[5] (Fig. 3a, e).

The proposed method achieved comparable ($n = 10$, 20.4% vs. $n = 11$, 24.2%[5]; No statistically significant difference) energy consumption reduction to state-of-the-art metabolism-driven CMA-ES optimizations[5,17]. (The apparent higher metabolic reduction in Slade et al.[17] was based on a bilateral ankle exoskeleton system. However, it[17] exhibited metabolic reduction capabilities equivalent to Zhang et al.[5], as verified by the same experimental study[17]. The method[17] was an efficient implementation of the latter[5] for metabolism minimization with the same optimization algorithm (CMA-ES) but a faster metabolism estimation process.) Notably, this result was attained while optimizing for reduction in joint torque, a local mechanical correlate to muscle activity, rather than whole-body energy cost. This suggests that maintaining user comfort throughout the optimization process may inherently support metabolic efficiency. Furthermore, our approach achieved state-of-the-art reductions in both metabolic cost and muscle activity with a single, 2-min optimization process, whereas prior approaches required separate protocols to minimize each metric individually[5,17].

Human joint mobility has been largely augmented. Due to the intention to minimize joint mechanical changes during optimization (Eq. (2)), and the fact that old and new assistance values were related by time index (Eq. (1)), the optimized assisted joint torque was close to the unassisted one on the axis of time within a stride (Fig. 4a). However, on the axis of joint angle, the assisted joint torque curve rose obviously from the unassisted one due to increased plantarflexion (Fig. 4b). It meant significantly more stride-wise input energy to human body, which appeared as decrease of negative power and increase of positive power during mid-stance (Fig. 4c, d). Increased joint power suggested improved local joint mobility.

The method's effectiveness across diverse ambulation conditions was attributed to its direct and exclusive reliance on human-optimized measurements of assisted and unassisted joint torque. The tuning rule (Eq. (1)) was constructed to be subtle and comfortable, guaranteeing the generation of physiologically meaningful joint torque profiles, regardless of gait conditions, assisted joints, assisting devices, and environments (treadmill and over-ground).

Easy deployment of the method to new scenarios arose from the non-parametric formulation, which required no pre-design and parameterization of exoskeleton assistance profiles. By deriving assistance directly from measured joint torques, the algorithm operated independently of ambulation conditions, eliminating the need for explicit gait identification. Transitioning to a new application scenario—whether due to changes in environment or user—simply required re-measuring baseline unassisted torque, identical to initial user calibration. This approach contrasts with traditional human-in-the-loop optimization methods[5,17], which necessitate extensive a priori research for specific joints, gait conditions, user populations, and exoskeleton devices.

The method's effectiveness when using ground reaction induced torque as joint torque estimates (τ_{joint}, Eq. (13)) demonstrated its robustness to estimation errors. In contrast, existing asssistance planning strategies based on joint moment usually employ complex estimation methods such as neural-network- or musculoskeletal-model-based ones[8,10,30] for better accuracy. The proposed method, though, used only the ground reaction data from the instrumented treadmill and position data of several motion markers (Eq. (12)). This tolerance was further confirmed by the successful implementation on the mobile exoskeleton outdoors, where ground reactions were estimated using one-dimensional pressure insole readings (Eq. (16)) rather than six-dimensional treadmill data. Additionally, the substitution of total joint torque (τ_{joint}) with human torque (τ_{human}) in the algorithm (Eq. (16)) suggested the framework's generalizability to alternative feedback modalities.

Performance relative to proportional-joint-torque approaches

The proposed update law (Eq. (1)) is characterized by an iterative tuning process and the steady-state convergence of exoskeleton torque to a portion of the steady-state assisted joint torque and one of the unassisted ($K_{dev} \cdot \tau_{joint} + K_{nom} \cdot \tau_{joint}^{ZT}$). Considering also that the method tries to minimize the difference between the two, this naturally leads to questions on its performance relative to strategies that direct asserting the same portions of real-time assisted joint torque ($\tau_{exo} = (K_{dev} + K_{nom}) \cdot \tau_{joint}$) or unassisted joint torque ($\tau_{exo} = (K_{dev} + K_{nom}) \cdot \tau_{joint}^{ZT}$).

The proposed iterative tuning method appeared to offer enhanced comfort, stability and effectiveness compared to approaches that formulates assistance directly from real-time joint moments or muscle activities[8,10,30,44]. Both strategies posit positive correlations between exoskeleton torque and human biomechanics, and thus may have performance dependent on the inner dynamics of how the human body reacts to intervention. However, our method implements a closed-loop optimization constrained around the baseline unassisted joint moment, whereas proportional-real-time-moment paradigms can be characterized as operating in a positive-feedback-loop manner. The proposed method (Eq. (1)) asserts minimal changes per stride and was designed to provide sufficient reaction time for human adaptation, which is hypothesized to promote comfort and cooperative responses. In contrast, proportional-moment approaches risk introducing abrupt intervention changes. Their efficacy, therefore, hinges on the user's ability to adapt cooperatively and instantaneously. Should a user respond defensively or adapt poorly, the system may enter vicious cycles with drifting and dangerous assistance. This interpretation was consistent with participant feedback describing the strategy as "difficult to control" and the observed lower muscle benefit compared to our method (35 ± 9.3% reduction from zero-torque condition for 0.5 gain, Supplementary Fig. 12, vs. 43.6 ± 12.7% in our method for participants with $K_{nom} + K_{dev} = 0.5$, Supplementary Fig. 5; the lack of statistical significance was likely due to small sample size). The inter-personal variability, coupled with observed user intolerance, suggested that the proportional joint torque strategy may be inherently unstable and sensitive to individual user dynamics and adaptation. Besides gradual adjustments, the presence of the nominal unassisted torque in the tuning rule was intended to prevent undesirable human reactions from destabilizing the system. Therefore, the heuristic optimization is suggested to be more robust and effective, particularly for users with gait impairments, ensuring both comfort and stability throughout adaptation.

Formulating assistance via the proposed iterative tuning appeared to lead to improved outcomes compared to directly applying a fixed portion of unassisted joint torque (Supplementary Fig. 13). The unassisted joint torque represents an equilibrium point resulting from the human user's adaptation to the exoskeleton's mechanical structure. Due to an imperfect human–machine interface, exoskeleton actuation cannot fully replace muscle actuation. Therefore, assisted joint torque is expected to inevitably deviate from the unassisted baseline as the system shifts to a new equilibrium under shared human-exoskeleton actuation (Fig. 4a). Different assistance profiles necessarily alter this equilibrium state. Within the resulting state space, one or several optimal equilibria may exist. The iterative tuning was intended to provide an efficient pathway to converge to such optima. In contrast, applying a fixed portion of the unassisted torque may fail to account for equilibrium shifts due to altered actuation modes and is therefore theorized to be inherently suboptimal. This provides a potential explanation why participants found the Gen2 condition uncomfortable, despite the low assistance torque and thus minimal difference in muscle benefit with optimized condition.

In summary, all three elements, i.e., the iterative process, the assisted joint torque, and the unassisted joint torque, are integral to the rule's effectiveness. The assisted torque enables closed-loop optimization that follows the user's internal adaptation. Iterative tuning nurtured cooperative human adaption. The assisted torque provides constrains and stability.

Advantages relative to all state-of-the-art planning methods

These features of the proposed method translate into some advantages distinguishing it from state-of-the-art exoskeleton assistance planning approaches[5,17,21,22].

Being explicit-model-based (Eq. (2)), it has rationally controllable optimization processes, theoretically explainable stability, and experimentally verified convergence to a fixed area with different optimization routes and speeds. These facilitate understanding and control of human-robot

interactions, which can potentially provide insights and options to better exoskeleton structure, interface and assistance designs. Meanwhile, current adaptive personalization methods[5,17] are model-free that take long (109 min[26]) to converge, but probably at different local extrema for different sessions; neural-network-based methods[21,22], on the other hand, are black boxes.

The method uses direct measurement of human-exoskeleton biomechanical interaction itself to influence and optimize interaction. While it is common in low-level control, e.g., torque tracking, to manipulate a variable by directly measuring, feeding back and influencing it, this is less explored for closed-loop exoskeleton high-level control. Current adaptive personalization methods[5,17] use indirect physiological signals as feedback, which lacks efficiency and precludes better understanding of human–robot coupling mechanism.

By being fast, comfortable and safe, this method is real-life accessible to various user groups. Current adaptive personalization processes require users to walk under multiple uncomfortable assistance profiles for at least 32 min. This is always undesirable for all users, unacceptable for a big portion, and impossible for the gait-impaired ones. On the other hand, instantaneous neural-network-based methods do not specifically attend to inter-personal differences or possible dangerous positive-feedback loops. Their safety and stability depend more on the ability of healthy users to quickly adapt to instant exoskeleton actions and stabilize the human-robot system. This creates risks in complex time-varying real-life scenarios, especially for gait-impaired users.

The proposed method is easily deployable at all stages. At the preparation stage of new applications: current adaptive personalization methods require pre-research to define and parameterize general assistance profiles; instantaneous neural-network-based methods require large experimental datasets, simulations and data training to form a black-box model. During the on-line assistance planning stage: current personalization methods need high computation power and actuation capacity to generate and realize randomized profiles; neural-network-based methods[21,22] require even higher power to run data-driven models. None of these applies to the rapid heuristic optimization. Moreover, it produces gentler assistance, which is safer and more energy-saving during actual assisted walking. Reduced research efforts, computing power and actuation capacity lead to easier re-planning and continuous planning, enduring battery usage and smaller motor sizes. Meanwhile, the non-parametric nature of the assistance and the simplicity of the method enable computational demands to scale linearly with the number of assisted joints, while optimization time remains unchanged. Thus, the method can be easily extended to multi-joint exoskeleton systems with only neglectable additional computing cost. All these suggest easier daily-life usage.

Conclusions and future works

The keys to the success of the proposed method, as discussed, included (a) an instantaneously measurable interaction-related feedback, (b) a reasonable tuning direction, and (c) a continuous direct association between the feedback and the variable to be optimized. We do not claim the necessity to choose assisted joint torque as feedback, or unassisted joint torque as nominal guide, or assistance torque as variable, or an updation rule based on absolute time in stride. Neither do we claim the necessity of matching data types between feedback and variable. Other interaction-related low-noise signals, such as interface impedance, power or energy, of the coupled system or a subsystem, might work as feedback. Sources other than experimental evaluations, such as simulations and prior studies, might be used to generate guides. Other forms of intervention to humans, such as admittance, impedance, or motion profiles, might work as variables. Updation of variables from prior values might be based on relative time in stride, kinetic information such as joint angles, or other kinds of gait phase estimators. Data-driven neural-network-based techniques might also be incorporated to enhance various parts of the process, e.g., joint torque estimation as in refs. 22,30. These and more possibilities are yet to be explored and verified. Further studies of the current implementation are also beneficial. For example, the best learning rates and optimization durations might differ for various applications[26]. Different relative weights between the nominal and the feedback terms in the guide might cause different behaviors and performances. The effects of torque estimation errors are not yet rigorously investigated. Insights of human–robot interaction and coupling mechanisms possibly revealed by the explicit model deserve deeper investigations. Moreover, the assistance profiles achieved through optimization under fairly fixed conditions can be generalized to practical scenarios with varying speeds and individual strides[53].

The proposed rapid optimization method significantly reduced research and operational costs for developers, physical and psychological costs for users, and time cost for both. It will largely elevate the accessibility level of effective, personalized and continuously-tuned practical exoskeletons in everyday scenarios and improve life quality for various users.

Methods

Interaction-based exoskeleton assistance tuning algorithm

The desired exoskeleton assistance torque started from a series of zeros (except the convergence tests) and was tuned iteratively at every stride based on the following rule:

$$\tau_{\mathrm{des}}(k, i+1) = (1-\alpha)\cdot\tau_{\mathrm{des}}(k, i) + \alpha\cdot[K_{\mathrm{nom}}\cdot\tau^{\mathrm{ZT}}_{\mathrm{joint}}(k) + K_{\mathrm{dev}}\cdot\tau_{\mathrm{joint}}(k, i)] \quad (1)$$

where τ_{des} is the desired assistance profile; k is the time index or the number of control cycles elapsed within this stride; i is the current stride number, and $i+1$ is the next; $\tau^{\mathrm{ZT}}_{\mathrm{joint}}$ is the pre-measured human joint moment when the participant walked wearing the exoskeleton but with zero assistance, i.e., unassisted joint torque; τ_{joint} is the real-time measured total joint moment of the coupled human-exoskeleton system, i.e., assisted joint torque; α is the learning rate, determining the update step size and convergence speed of the assistance profile; K_{nom} and K_{dev} are coefficients of the nominal part and feedback part respectively; $[K_{\mathrm{nom}}\cdot\tau^{\mathrm{ZT}}_{\mathrm{joint}}(k) + K_{\mathrm{dev}}\cdot\tau_{\mathrm{joint}}(k, i)]$ together forms a tuning guide that directs the tuning process.

Analysis of gradient descent rapid heuristic optimization

This tuning algorithm realized a gradient descent optimization process, composed of a series of independent sub-processes, that minimizes the combined cost of human biological joint moment, exoskeleton assistance and the deviation of total assisted joint torque from the unassisted human joint torque.

Consider a stride-wise cost function $J_{\mathrm{stride}} = \sum_{k=1}^{\mathrm{StrideEnd}} J(k)$, in which $J(k)$ stands for the cost function for index k within the gait cycle, formulated as

$$J(k) = \frac{1}{2}\lambda_1(k)\tau^2_{\mathrm{human}}(k) + \frac{1}{2}\lambda_2(k)\tau^2_{\mathrm{exo}}(k) + \frac{1}{2}\lambda_3(k)[\tau_{\mathrm{joint}}(k) - \tau^{\mathrm{ZT}}_{\mathrm{joint}}(k)]^2. \quad (2)$$

τ_{human} is the human biological joint moment, τ_{exo} is the exoskeleton assistance torque, τ_{joint} is the human-exoskeleton combined joint moment, $\tau^{\mathrm{ZT}}_{\mathrm{joint}}$ is the unassisted human joint torque. The coefficients $\lambda_1(k), \lambda_2(k), \lambda_3(k)$ are non-negative and remain fixed for each specific index k.

The partial derivative of the cost function with respect to τ_{exo} is

$$\frac{\partial J(k)}{\partial\tau_{\mathrm{exo}}(k)} = \lambda_1(k)\tau_{\mathrm{human}}(k)\cdot\frac{\partial\tau_{\mathrm{human}}(k)}{\partial\tau_{\mathrm{exo}}(k)} + \lambda_2(k)\tau_{\mathrm{exo}}(k) + \lambda_3(k)[\tau_{\mathrm{joint}}(k) - \tau^{\mathrm{ZT}}_{\mathrm{joint}}(k)]\cdot\frac{\partial\tau_{\mathrm{joint}}(k)}{\partial\tau_{\mathrm{exo}}(k)} \quad (3)$$

Since $\tau_{\mathrm{joint}}(k) = \tau_{\mathrm{human}}(k) + \tau_{\mathrm{exo}}(k)$,

$$\frac{\partial\tau_{\mathrm{human}}(k)}{\partial\tau_{\mathrm{exo}}(k)} = \frac{\partial\tau_{\mathrm{joint}}(k)}{\partial\tau_{\mathrm{exo}}(k)} - 1. \quad (4)$$

Let $\rho(k) = \frac{\partial \tau_{joint}(k)}{\partial \tau_{exo}(k)}$, we have

$$\begin{aligned}\frac{\partial J(k)}{\partial \tau_{exo}(k)} &= \lambda_1(k)\tau_{human}(k)\cdot[\rho(k)-1] + \lambda_2(k)\tau_{exo}(k) + \lambda_3(k)\left[\tau_{joint}(k) - \tau^{ZT}_{joint}(k)\right]\cdot\rho(k) \\ &= \left[\lambda_2(k) - \lambda_1(k)\rho(k) + \lambda_1(k)\right]\tau_{exo}(k) + \left[\lambda_1(k)\rho(k) - \lambda_1(k)\right]\tau_{joint}(k) \\ &\quad + \lambda_3(k)\rho(k)\left[\tau_{joint}(k) - \tau^{ZT}_{joint}(k)\right].\end{aligned} \tag{5}$$

By gradient descent and the assumption that $\tau_{exo} = \tau_{des}$, with a learning rate of $\lambda(k)$,

$$\begin{aligned}\tau_{exo}(k, i+1) &= \tau_{exo}(k, i) - \lambda(k)\cdot\frac{\partial J(k)}{\partial \tau_{exo}(k)} \\ &= \left\{1 - \lambda(k)\left[\lambda_2(k) - \lambda_1(k)\rho(k) + \lambda_1(k)\right]\right\}\tau_{exo}(k, i) \\ &\quad + \lambda(k)\lambda_1(k)\left[1-\rho(k)\right]\tau_{joint}(k, i) + \lambda(k)\lambda_3(k)\rho(k) \\ &\quad \left[\tau^{ZT}_{joint}(k) - \tau_{joint}(k, i)\right].\end{aligned} \tag{6}$$

Human locomotion is itself optimized and tends to maintain its original biomechanics as much as possible in the presence of external disturbances. Especially under gentle assistance tuning like the approach in this study, in which $\alpha = 0.025$ and $K_{nom} + K_{dev} < 1$, human feels rather comfortable and safe and will not overreact[51], i.e., $|\rho| \ll 1$ (Supplementary Fig. 14).

Here, negative, zero and positive ρ values respectively indicate that muscle torque reduction is a bit more than, the same as and slightly less than exoskeleton input increase. In any of these cases, total joint torque is not largely affected while human effort is partially replaced by exoskeleton at an efficiency R (Eq. (7)) of about 100%.

$$R = \frac{-\partial \tau_{human}}{\partial \tau_{exo}} \times 100\% = 1 - \rho \tag{7}$$

Any exoskeleton intervention that causes more improvement of mobility than the increase of human efforts constitutes meaningful assistance. Hundred percent R clearly represents one such instance.

Meanwhile, the tendency to keep natural joint biomechanics, ensured by complex human dynamics, also means a larger coefficient for joint torque changes, λ_3, relative to λ_1 and λ_2, in the cost function.

The approach proposed in this study was equivalent to enforcing a small constant positive $\rho(k)$, and thus constant α, K_{nom} and K_{dev} values at index k for an optimization session. Rewriting Eq. (6), we got the assistance update algorithm in the format of Eq. (1) as below:

$$\begin{aligned}\tau_{exo}(k, i+1) &= (1-\alpha)\tau_{exo}(k, i) + \alpha(K_{dev} + K_{nom})\tau_{joint}(k) \\ &\quad + \alpha K_{nom}\left[\tau^{ZT}_{joint}(k) - \tau_{joint}(k, i)\right] \\ &= (1-\alpha)\tau_{exo}(k, i) + \alpha\left[K_{nom}\tau^{ZT}_{joint}(k) + K_{dev}\tau_{joint}(k, i)\right]\end{aligned} \tag{8}$$

in which

$$\begin{aligned}\alpha &= \lambda(k)[\lambda_2(k) - \lambda_1(k)\rho(k) + \lambda_1(k)], \\ K_{dev} + K_{nom} &= \frac{\lambda_1(k)[1-\rho(k)]}{\lambda_2(k) - \lambda_1(k)\rho(k) + \lambda_1(k)} \in (0, 1), \\ K_{nom} &= \frac{\lambda_3(k)\rho(k)}{\lambda_2(k) - \lambda_1(k)\rho(k) + \lambda_1(k)} > 0.\end{aligned} \tag{9}$$

Analysis based on the cost function in Eq. (2) aligns with that based on the tuning rule in Eq. (1). Equal weights of nominal and feedback terms in tuning guide, i.e., $K_{nom} = K_{dev}$, together with a small $\rho(k)$, means a big $\lambda_3(k)$, which aligns with previous discussion that small $\rho(k)$ and big $\lambda_3(k)$ come as a pair. For example, $\lambda_3(k) = 9.5\lambda_1(k)$ when $\rho(k) = 0.05$. Meanwhile, smaller K_{nom} and K_{dev} values suggest larger $\lambda_2(k)$, i.e., more intention to keep exoskeleton assistance smaller. This aligned with the results that participants with smaller K_{nom} and K_{dev} had smaller peak optimized torque values (Supplementary Table 2 and Supplementary Fig. 11).

*More on ρ, *R* and human–exoskeleton interaction behavior. Both $\rho = \frac{\partial \tau_{joint}}{\partial \tau_{exo}}$ and $R = -\frac{\partial \tau_{human}}{\partial \tau_{exo}}$ describe human body's reactions to exoskeleton input. They are governed by the internal physical and chemical dynamics of human body. The definition of ρ was introduced to design, by inverse dynamics, an exoskeleton torque tuning rule (Eq. (1)) that governs how the exoskeleton reacts to human actions, i.e., $\frac{\partial \tau_{exo}}{\partial \tau_{joint}}$ or $\frac{\partial \tau_{exo}}{\partial \tau_{human}}$. Therefore, the values of ρ solely without the knowledge of $\frac{\partial \tau_{exo}}{\partial \tau_{joint}}$, sometimes cannot fully portray the human-exoskeleton interaction behaviors.

When $|\rho| \ll 1$, as produced by the proposed method in this study, human effort is replaced by exoskeleton at an efficiency of $R \approx 100\%$. This qualifies as effective exoskeleton assistance while maintaining original mobility. In this region, $-1 \ll \rho < 0$, $\rho = 0$ and $0 < \rho \ll 1$ correspond to slight reduction, maintenance, and slight augmentation of the total joint torque, respectively.

Beyond the $|\rho| \ll 1$ region and discussion of this rapid heuristic optimization method, if $0 < \rho \le 1$ ($0 \le R < 100\%$), an increase in exoskeleton torque causes a decrease or no change in human torque. Total joint torque is thus augmented.

If $\rho > 1$, an increase in exoskeleton torque will lead to an increase in human torque, which means the user is resisting exoskeleton intervention. Although joint torque is further enlarged, this situation may incur instability and endanger the user, depending on the exoskeleton high level controller for input torque planning, i.e., $\frac{\partial \tau_{exo}}{\partial \tau_{joint}}$.

If $\rho < 0$ (i.e., $R > 100\%$), the user feels insecure and attempts to disengage or 'escape' from the exoskeleton. Human torque decreases more than exoskeleton torque increases, leading to a net reduction in total joint torque.

However, this analysis is about instant changes in total joint torque. To fully assess joint mobility and human-exoskeleton interaction modes, changes in joint torque and joint motion must be considered together over the entire gait cycle.

Experimental protocol and participants

We performed five sets of experimental studies to test our method. The main one was to test the effectiveness of the proposed method across individuals. The single-subject generality studies were to verify the effectiveness of the method across gait conditions, assisting devices and assisted joints, and to demonstrate the ease in deploying new applications. Single-subject convergence tests were to investigate the influence of learning rates and initial positions on optimization results. We tested the performance of exoskeleton torque proportional to real-time total joint torque. We also compared the performance of our proposed method against applying a proportional share of baseline unassisted joint torque. All experimental protocols were approved by Nankai University Biological and Medical Ethics Committee (No. NKUIRB2023058). All participants provided written informed consents before the experiments.

Ten healthy individuals (8 males and 2 females; age = 23.8 ± 1.0 [23–26] years; mass = 68.2 ± 8.4 [51–83] kg; height = 1.74 ± 0.06 [1.65–1.88] m; mean ± standard deviation [range]. Supplementary Table 1) participated in the main study. Participants wore a tethered unilateral single-degree-of-freedom ankle exoskeleton (Fig. 2c and Supplementary Fig. 1) that provided plantarflexion assistance during treadmill walking at 1.25 m s^{-1}. All participants experienced two experimental stages: optimization and validation. Before optimization, each new participant put on the exoskeleton, walked in it with zero assistance, and tried to walk under some experience-based assistance profiles with ramping peak torques. This familiarization process took several minutes. Stable walking joint moments under zero-torque mode were recorded for ten strides and averaged to evaluate unassisted joint torques. The value of $K_{dev} = K_{nom}$ for the

optimization was set based on the amount of assistance the participant was willing to tolerate ([0.175, 0.25]).

During optimization, each participant started walking with a desired exoskeleton assistance torque profile consisting of a series of zeros. It was then tuned stride-wise towards the real-time measured ankle torque and nominal unassisted joint torque based on Eq. (1), with a learning rate $\alpha = 0.025$, for 2 min. The assistance at the end was considered the optimized assistance. In validation, participants walked under the optimized condition and the control conditions. All participants walked with normal-shoe and zero-torque control conditions. Seven of the ten also walked with a generic control condition achieved by averaging the optimized profiles of a state-of-the-art approach[5] (0.74 Nm kg^{-1} peak torque, 50.4% peak time, 22.8% rise time, and 12.8% fall time, Fig. 3h). The remaining three participants skipped the generic assistance since they found it unbearable. All conditions were tested in a double-reversal order of NW (normal-shoe walking)–ZT (zero-torque mode)–Gen (generic assistance mode)–Opt (optimized assistance mode)–Opt–Gen–ZT–NW. Each session lasted 6 min.

Placing the NW condition at both ends eliminated the need for multiple donning and doffing cycles. It ensured a consistent human-device interface for all exoskeleton-involved conditions (ZT, Gen, Opt) in between and thus a cleaner comparison. The Opt condition was positioned centrally to maximize the time gap between the end of the optimization process and the validation of Opt condition. This design deliberately counteracts the potential advantage Opt could gain from short-term human adaptation and familiarity during the prior iterative tuning, ensuring a fairer comparison against other conditions. ZT was tested before Gen as it represents a more distinct departure from the Opt condition. This sequence further helped to "defamiliarize" the user from the Opt condition before testing the more similar Gen profile.

Metabolic consumption, muscle activity and kinematics were measured throughout the process. Data of the last 3 min were averaged between two sessions of repeated conditions for analysis (Figs. 3 and 4; Supplementary Figs. 5–10). All participants completed their trials within 2 h on their respective experiment day.

Six participants were recruited to evaluate the high-level exoskeleton planning strategy the asserts assistance proportional to the real-time estimates total joint torque, i.e.,

$$\tau_{exo} = K_f \cdot \tau_{joint} \tag{10}$$

where K_f is the proportional ratio, on the same unilateral ankle exoskeleton emulator as the main study. Two were unable to complete the protocol due to intolerance of the exoskeleton-induced instability. Consequently, data from four participants (all male, 24.3 ± 0.96 years, 1.83 ± 0.05 m, 72.8 ± 8.4 kg; Supplementary Table 3) were included in the analysis. Three participants (P2, P7, P12) completed trials at gains of $K_f = [0.2, 0.3, 0.4, 0.5]$. The fourth participant (P11) could not tolerate the $K_f = 0.5$ condition. ZT condition was included in validation as a reference. Conditions were tested in the order of ZT–$0.2\tau_{joint}$–$0.3\tau_{joint}$–$0.4\tau_{joint}$–$0.5\tau_{joint}$–$0.5\tau_{joint}$–$0.4\tau_{joint}$–$0.3\tau_{joint}$–$0.2\tau_{joint}$–ZT.

3 participants (all male, 24.7 ± 1.5 years, 1.79 ± 0.08 m, 76.3 ± 8.4 kg; Supplementary Table 4) were recruited for the comparison between the proposed method to the second generic assistance (Gen2), which asserted assistance proportional to the joint torque during zero-torque mode, i.e.,

$$\tau_{exo} = K_p \cdot \tau_{joint}^{ZT} \tag{11}$$

where K_p is a constant ratio. Tests were conducted on the same unilateral ankle exoskeleton emulator. While two participants (P14, P6) used relatively small pre-set gains ($K_p = 0.35$, $K_{dev} = K_{nom} = 0.175$), the third (P2) self-selected the maximum gains he was willing to tolerate for both conditions: $K_p = 0.4$ for Gen2 and $K_{dev} = K_{nom} = 0.5$ for the optimized case. ZT condition was included in validation for references. Conditions were tested in the order of ZT–Gen2–Opt–Opt–Gen2–ZT.

One individual (P1) participated in all generality studies. The method was tested for the same unilateral ankle exoskeleton as main study when level walking speed changed from low (1.0 m s^{-1}), medium (1.25 m s^{-1}), to high (1.5 m s^{-1}), terrain changed to uphill (10° incline, 1.25 m s^{-1}), loaded was added to human body (20% body mass, 1.25 m s^{-1}) and gait changed to running (2.5 m s^{-1}). It was also tested when assisted device changed to a bilateral exoskeleton (1.25 m s^{-1}, level walking, Fig. 2c), a knee exoskeleton (5° uphill walking, 1.25 m s^{-1}, Fig. 2d and Supplementary Fig. 3) and a mobile unilateral ankle exoskeleton (outdoor ground level walking, preferred speed, Fig. 2e and Supplementary Fig. 2). The optimization and validation processes were similar to those of main study. In unilateral ankle exoskeleton studies, the normal-shoe mode was used as a control condition in validation. For the bilateral ankle exoskeleton and knee exoskeleton, control conditions were normal-shoe and zero-torque. In the case of knee assistance, rectus femoris muscle activity was measured instead of the soleus. For the mobile exoskeleton outdoors, the control condition was zero-torque and only muscle activity was measured in validation. All studies with the unilateral ankle exoskeleton were conducted within a single day. The participant had 20-min breaks in between conditions. We tested the method on the bilateral ankle exoskeleton and the unilateral knee exoskeleton on a different day, and the mobile ankle exoskeleton on another.

P1 also walked for the optimization convergence studies of different learning rates and initial states. They were with the same exoskeleton and walking speed as the main study. These studies included only optimization without validation sessions. For the learning rate study, the participant started with zero assistance and had the assistance tuned with 5 different rates ($\alpha = \{0.005, 0.01, 0.025, 0.05, 0.1\}$). The influence of the initial assistance profile was tested by setting it as nine different curves instead of zeros. These curves were generated by the combination of three peak times (47%, 50%, and 53%) and three peak torques (20 Nm, 40 Nm, 60 Nm) with the same rise and fall times as the generic condition[5].

Exoskeleton hardware and control

All experimental studies except the one on mobile ankle exoskeleton were conducted with a tethered exoskeleton emulator comprising a wearable exoskeleton end-effector and an off-board actuation and control module (Fig. 2a–d and Supplementary Fig. 1).

The unilateral ankle exoskeleton end-effector[47] in the main, generality, and convergence studies can provide plantarflexion torque assistance during walking or running (Fig. 2b). It consists of shank, foot and heel segments, with most parts machined from carbon fiber or 7075 aluminum. The end-effector weighs 0.5 kg and can provide assistance torques up to 100 Nm. Flexible Bowden cable connects the end-effector and off-board actuator, delivering assistance forces and powers. Force is transmitted to the user beneath the heel by a rope and below the knee via a padded strap. The end-effectors of the bilateral ankle exoskeleton used in the generality study were modified from the unilateral one[50]. The shank carbon fiber struts were redesigned as a hook shape. Their posterior sides were rotated about the longitudinal axis towards the human leg for 10 ° to avoid possible contacts between the legs during walking. Other parts were also adjusted for better comfort and safety.

The unilateral knee exoskeleton end-effector, inspired by a previous design[54], consists of the thigh and the shank segments (Supplementary Fig. 3). It interfaces with the user behind the thigh, below the knee and above the ankle by wraps, providing extension assistance to the knee joint. Similar to the ankle exoskeleton end-effectors, a U-shaped patella bracket sits in front of the knee to connect the driving cable. Machined by carbon fiber, it has a long lever arm and provides series elasticity. The thigh and shank carbon fiber struts also have an internal rotation at the posterior side to avoid collision between assisted and unassisted legs. The knee exoskeleton end-effector weighs 0.86 kg in total.

Three types of sensors were integrated into each of the end-effectors. A load cell (DYMH-106, DAYSENSOR, China) was fixed at the end of the driving cable to measure the assistance force. Assistance torque was

calculated by multiplying the measured force and lever arm of the end-effector. A magnetic encoder (PQY18, ACCNT, China) was installed on the joint axle to sense the joint angle. Heel strikes were detected by a foot switch (KW12, Risym, China) attached to the lateral side of the shoe on the assisted leg for detecting gait cycles. A signal-bridging module between the sensors and an assembled data cable was designed and installed to ease switching of end-effectors.

Off-board actuation and control module provided a wide range of assistance and accurate torque tracking. The actuation system comprised an AC servo motor, a 5:1 planetary gear mechanism and a motor driver (BSM90N-175AA, GBSM90-MRP120-5, and MF180-04AN-16 A, ABB, Switzerland). A real-time controller (MicroLabBox, dSPACE, Germany) acquired sensor signals at 5000 Hz and executed exoskeleton planning and control at 500 Hz. To assist human locomotion, exoskeletons enforced assistance profiles by a combination of proportional-derivative control, model-based feed-forward control and iterative learning control[49] during the stance phase. In the swing phase of assistance mode and both phases of zero-torque mode, exoskeletons followed the wearer's joint movements.

Real-time biomechanics estimation

The rapid heuristic exoskeleton assistance optimization relied on the real-time measurement of human-exoskeleton joint biomechanics. We estimated the total joint moment as the torque produced by the ground reaction force (GRF) on the human joint axis by ignoring joint inertia and acceleration[55].

In all studies except the outdoor mobile ankle exoskeleton one, GRF was measured by an instrumented split-belt treadmill (FIT, Bertec, USA). Ten motion capture cameras measured kinematic data (Oqus 700, Qualisys, Sweden). During ankle exoskeleton assistance, two optical markers were affixed on the medial and lateral sides of the assisted ankle joint to instruct the joint axis (Supplementary Fig. 4). The real-time controller (MicroLabBox, dSPACE, Germany) collected the GRF data through analog acquisition, and marker coordinates through Ethernet communication at 500 Hz. The signals were then low-pass filtered at 25 Hz before calculation.

The measured coordinates of lateral joint marker Pt_{l}, medial joint marker Pt_{m}, the center of pressure Pt_{cop} and the GRF $\vec{F}_{\mathrm{grf}}$ were represented as:

$$Pt_{\mathrm{l}}=\begin{bmatrix}x_{\mathrm{l}}\\ y_{\mathrm{l}}\\ z_{\mathrm{l}}\end{bmatrix},\ Pt_{\mathrm{m}}=\begin{bmatrix}x_{\mathrm{m}}\\ y_{\mathrm{m}}\\ z_{\mathrm{m}}\end{bmatrix},\ Pt_{\mathrm{cop}}=\begin{bmatrix}x_{\mathrm{cop}}\\ y_{\mathrm{cop}}\\ z_{\mathrm{cop}}\end{bmatrix},\ \vec{F}_{\mathrm{grf}}=\begin{bmatrix}F_{\mathrm{x}}\\ F_{\mathrm{y}}\\ F_{\mathrm{z}}\end{bmatrix}. \quad (12)$$

The total joint torque (moment) was then estimated as:

$$\begin{aligned}\tau_{\mathrm{joint}}&=(\vec{r}\times\vec{F}_{\mathrm{grf}})\cdot\vec{e}_{\mathrm{axis}}\\&=(r_{\mathrm{y}}F_{\mathrm{z}}-r_{\mathrm{z}}F_{\mathrm{y}})e_{\mathrm{x}}+(r_{\mathrm{z}}F_{\mathrm{x}}-r_{\mathrm{x}}F_{\mathrm{z}})e_{\mathrm{y}}+(r_{\mathrm{x}}F_{\mathrm{y}}-r_{\mathrm{y}}F_{\mathrm{x}})e_{\mathrm{z}}\end{aligned} \quad (13)$$

where

$$\vec{r}=\overrightarrow{Pt_{\mathrm{l}}Pt_{\mathrm{cop}}}=\begin{bmatrix}x_{\mathrm{cop}}-x_{\mathrm{l}}\\ y_{\mathrm{cop}}-y_{\mathrm{l}}\\ z_{\mathrm{cop}}-z_{\mathrm{l}}\end{bmatrix}=\begin{bmatrix}r_{\mathrm{x}}\\ r_{\mathrm{y}}\\ r_{\mathrm{z}}\end{bmatrix} \quad (14)$$

and the unit vector along the joint axis from medial to lateral side is

$$\vec{e}_{\mathrm{axis}}=\frac{\overrightarrow{Pt_{\mathrm{l}}Pt_{\mathrm{m}}}}{|\overrightarrow{Pt_{\mathrm{l}}Pt_{\mathrm{m}}}|}=\begin{bmatrix}\frac{x_{\mathrm{m}}-x_{\mathrm{l}}}{\sqrt{(x_{\mathrm{m}}-x_{\mathrm{l}})^2+(y_{\mathrm{m}}-y_{\mathrm{l}})^2+(z_{\mathrm{m}}-z_{\mathrm{l}})^2}}\\ \frac{y_{\mathrm{m}}-y_{\mathrm{l}}}{\sqrt{(x_{\mathrm{m}}-x_{\mathrm{l}})^2+(y_{\mathrm{m}}-y_{\mathrm{l}})^2+(z_{\mathrm{m}}-z_{\mathrm{l}})^2}}\\ \frac{z_{\mathrm{m}}-z_{\mathrm{l}}}{\sqrt{(x_{\mathrm{m}}-x_{\mathrm{l}})^2+(y_{\mathrm{m}}-y_{\mathrm{l}})^2+(z_{\mathrm{m}}-z_{\mathrm{l}})^2}}\end{bmatrix}=\begin{bmatrix}e_{\mathrm{x}}\\ e_{\mathrm{y}}\\ e_{\mathrm{z}}\end{bmatrix}. \quad (15)$$

Joint moments determined this way have negligible differences from those calculated using inverse dynamics[55]. The method has been adopted in various exoskeleton applications[56].

To measure the joint angle, another two markers were affixed on the lateral side of two adjacent joints, such as the knee and metatarsophalangeal joints for the ankle. Joint angle measurements were calibrated during quiet standing. Joint powers were calculated by multiplying measured joint moments and velocities.

Outdoor exoskeleton assistance optimization

We tested the proposed method during outdoor level ground walking with a mobile unilateral ankle exoskeleton. The mobile exoskeleton consists of a right ankle end-effector, a waist actuation pack and a portable lithium battery (Supplementary Fig. 2). The whole system weighs 2.5 kg, of which the end-effector 0.45 kg. The end-effector is the same as the one used in the tethered bilateral ankle exoskeleton[50] in the generality study. The actuation system was attached to the back of the waist to reduce distal mass and metabolic penalty. A 24 V, 4700 mAh lithium battery (TB47S, DJI, China) powered the mobile exoskeleton system, allowing 3 h of continuous assisted walking.

The waist actuation pack comprises motors, driving cable transmission assemblies, and an embedded controller (Supplementary Fig. 2a). Two brushless DC geared motors (CyberGear, Xiaomi, China) were mounted in the actuation pack with only one used in this study. Each motor weighs 0.32 kg and has a rated peak torque of 12 Nm with no-load speed of 296 rpm. A customized pulley with a radius of 0.020 m connects the driving cable to the end-effector's heel bracket, which produces a 5:1 driving ratio and provides a peak torque of 60 Nm at the assisted ankle. A control circuit board with two embedded microcontroller units (i.e., MCU; ESP32-WROOM32D, Espressif, China) was developed for real-time control and assistance optimization. One MCU is the controlling unit performing sensor data collection and closed-loop control at 500 Hz. The other is the planning unit performing profile generation and optimization. Meanwhile, it communicated with the host PC by wireless network, sending exoskeleton states and receiving operation commands. The entire waist actuation pack weighs 1.2 kg.

An instrumented pressure insole was used to estimate the biological ankle moment during outdoor walking (Supplementary Fig. 2e). An acquisition unit scanned the arrayed pressure sensors of the filmy insole (RXES42-16P, Roxifsr, China) and transmitted all 8 sensors' pressure readings Pr_j (j={1,2,...,8}; Supplementary Fig. 2n) to the planning MCU through wireless network at 500 Hz. Since the foot pressure insole was installed inside the shoe, total joint torque was not available as in in-lab tests. Instead, only the human biological ankle joint moment was estimated, as:

$$\tau_{\mathrm{human}}=\sum_{j=1}^{8}r_jS_jPr_j \quad (16)$$

where r_j was the distance from the center of the j-th pressure sensor to the ankle joint axis; S_j was the area coefficient of j-th pressure sensor. Parameters were calibrated by the joint moments calculated using the OpenSim inverse dynamics tool from the data measured by the instrumented treadmill and motion capture cameras.

One participant (P1) walked for the outdoor assistance optimization pilot tests. The participant wore the ankle exoskeleton on his right foot and walked outside along a flat path with a preferred speed. The unassisted joint moment $\tau_{\mathrm{joint}}^{\mathrm{ZT}}$ was measured with the exoskeleton providing zero assistance torque before the optimization stage. Then the assistance profile was iteratively tuned by the unassisted joint moment and real-time estimated biological moments as

$$\begin{aligned}\tau_{\mathrm{des}}(k,i+1)=(1-\alpha)\cdot\tau_{\mathrm{des}}(k,i)+\alpha\cdot[K_{\mathrm{nom}}\cdot\tau_{\mathrm{joint}}^{\mathrm{ZT}}(k)\\+K_{\mathrm{dev}}\cdot\tau_{\mathrm{human}}(k,i)].\end{aligned} \quad (17)$$

It was different from the algorithm of in-lab studies (Eq. (1)) by using human joint torque $\tau_{human}(k)$, instead of total joint torque $\tau_{joint}(k)$, as feedback. α, K_{nom}, K_{dev} had the same definition as those in the tethered system. The latter two were set as 0.175 in the outdoor experiment, and α was 0.025. After a 2-min optimization, the assistance was evaluated compared to the zero-torque condition in a double-reversal order (ZT-Opt-Opt-ZT).

Validation data collection and processing

Metabolic energy consumption and electromyography were recorded to evaluate the effectiveness of the optimized assistance in the main and generality studies. Participants were told to refrain from all food and drink except water for at least 3 h before experiments. Metabolic consumption was indirectly measured through breath-by-breath carbon dioxide and oxygen volumes through respiratory equipment (K5, Cosmed, Italy). It was computed with a standard equation[57] and averaged over the last 3 min of each trial of validation. Net metabolic cost was calculated as the steady-state metabolic cost minus the quiet standing metabolic cost, which was measured before validation tests during a quiet standing session.

Muscle activities were measured by surface electromyography (Trigno, Delsys, USA), and the signals were acquired at 500 Hz by the real-time controller. The raw signals were processed through a 25 Hz high-pass filter, a rectifier, and a 6 Hz low-pass filter to produce clearer envelopes. The EMG envelopes were averaged across strides of the last 3 min of each condition and normalized by the peak magnitude of the related control condition for each participant (Figs. 3g and 5e–h). The Root-Mean-Square (RMS) of stride-wise EMG envelopes was calculated and averaged across strides to reflex the average muscle activation (Figs. 3a, c and 5i–l). For the main study, RMS soleus muscle activity was normalized by each participant's normal-shoe mode. During the in-lab generality studies, RMS local muscle activity of each gait condition was normalized by the normal-shoe condition of medium speed level walking for unilateral ankle exoskeleton tests (Fig. 5i), normal-shoe condition for bilateral ankle exoskeleton (Fig. 5j) and knee exoskeleton (Fig. 5k), and zero-torque condition for mobile exoskeleton outdoors (Fig. 5l).

For all the data presented along the axis of time or angle (Figs. 3g, h, 4a–c, and 5a–f; Supplementary Figs. 7–9), the measured data of each stride were off-line resampled to the same length of 1000, averaged across all strides, and again averaged across participants when necessary. Metabolic costs, joint moments, joint mechanical power, assistance profiles, and assisted power were normalized by the body mass of each participant for the purpose of comparison. The reductions in metabolic costs and muscle activities were calculated as percentages and averaged across all participants.

For tests on bilateral plantarflexion ankle exoskeleton, independent optimizations were conducted for two legs. In validation, muscle activities and biomechanics were measured independently for two legs and averaged for presentation (Fig. 5b, f, j, n).

Statistical analysis

For metabolic consumption, RMS muscle activities and stride-wise joint power in the main study, we reported the statistical difference between validation conditions. All statistical analyses were performed with MATLAB R2023b after experiments. We used paired *t*-tests to compare the optimized assistance condition with generic assistance ($n = 7$), normal-shoe ($n = 10$), and zero-torque conditions ($n = 10$). The significant level was 0.05 for all analyses. No statistical analysis was performed for additional generality experiments of a small sample size ($n = 1$). Two-tailed unpaired *t*-tests were used to compare the performance of our method demonstrated by the main study, including optimized assistance parameters, metabolic cost reduction and muscle activities reduction,with a control study[5]. In the proportional joint moment study, paired *t*-tests were used to compare each of the four conditions and zero-torque on stride-wise positive work and soleus activity, Holm–Bonferroni correction on *P* values was used to control family-wise error rate of type I errors. The eight *P* values from paired *t*-tests of the main study were adjusted as a family. The three from unpaired *t*-tests between the optimized condition in our study and that in literature[5] were adjusted as a second family. The 8 from paired *t*-tests of the proportional-moment study were adjusted as a third family. The two from paired *t*-tests for the comparison between optimized condition and the generic assistance proportional to unassisted joint torque were adjusted as a fourth family.

Data availability

All data supporting the findings of this study, as presented in texts, figures and tables, are available in Supplementary Data 1 in Matlab.mat format. Readme files explaining the data structure and sample access codes are also included in S1. Experimental procedures and testbed setups are shown in Supplementary Movie 1.

Code availability

Example scripts are provided in Supplementary Data 1 to exhibit how to process the data. This code uses Matlab version 2023b.

Received: 1 April 2025; Accepted: 11 December 2025;
Published online: 30 December 2025

References

1. Dollar, A. M. & Herr, H. Lower extremity exoskeletons and active orthoses: challenges and state-of-the-art. *IEEE Trans. Robot.* **24**, 144–158 (2008).
2. Sawicki, G. S., Beck, O. N., Kang, I. & Young, A. J. The exoskeleton expansion: improving walking and running economy. *J. NeuroEng. Rehabil.* **17**, 25 (2020).
3. Siviy, C. et al. Opportunities and challenges in the development of exoskeletons for locomotor assistance. *Nat. Biomed. Eng.* **7**, 456–472 (2023).
4. Veneman, J. F. et al. Design and evaluation of the lopes exoskeleton robot for interactive gait rehabilitation. *IEEE Trans. Neural Syst. Rehabil. Eng.* **15**, 379–386 (2007).
5. Zhang, J. et al. Human-in-the-loop optimization of exoskeleton assistance during walking. *Science* **356**, 1280–1284 (2017).
6. Awad, L. N. et al. A soft robotic exosuit improves walking in patients after stroke. *Sci. Transl. Med.* **9**, eaai9084 (2017).
7. Kim, J. et al. Reducing the metabolic rate of walking and running with a versatile, portable exosuit. *Science* **365**, 668–672 (2019).
8. Gasparri, G. M., Luque, J. & Lerner, Z. F. Proportional joint-moment control for instantaneously adaptive ankle exoskeleton assistance. *IEEE Trans. Neural Syst. Rehabil. Eng.* **27**, 751–759 (2019).
9. Witte, K. A., Fiers, P., Sheets-Singer, A. L. & Collins, S. H. Improving the energy economy of human running with powered and unpowered ankle exoskeleton assistance. *Sci. Robot.* **5**, eaay9108 (2020).
10. Durandau, G., Rampeltshammer, W. F., van der Kooij, H. & Sartori, M. Neuromechanical model-based adaptive control of bilateral ankle exoskeletons: biological joint torque and electromyogram reduction across walking conditions. *IEEE Trans. Robot.* **38**, 1380–1394 (2022).
11. Kim, J. et al. Soft robotic apparel to avert freezing of gait in parkinson's disease. *Nat. Med.* **30**, 177–185 (2024).
12. Tricomi, E. et al. Soft robotic shorts improve outdoor walking efficiency in older adults. *Nat. Mach. Intell.* **6**, 1145–1155 (2024).
13. Malcolm, P., Derave, W., Galle, S. & De Clercq, D. A simple exoskeleton that assists plantarflexion can reduce the metabolic cost of human walking. *PloS ONE* **8**, e56137 (2013).
14. Mooney, L. M., Rouse, E. J. & Herr, H. M. Autonomous exoskeleton reduces metabolic cost of human walking during load carriage. *J. NeuroEng. Rehabil.* **11**, 80 (2014).
15. Collins, S. H., Wiggin, M. B. & Sawicki, G. S. Reducing the energy cost of human walking using an unpowered exoskeleton. *Nature* **522**, 212–215 (2015).
16. Ding, Y., Kim, M., Kuindersma, S. & Walsh, C. J. Human-in-the-loop optimization of hip assistance with a soft exosuit during walking. *Sci. Robot.* **3**, eaar5438 (2018).

17. Slade, P., Kochenderfer, M. J., Delp, S. L. & Collins, S. H. Personalizing exoskeleton assistance while walking in the real world. *Nature* **610**, 277–282 (2022).
18. Schmitz, D. G. et al. Modulation of achilles tendon force with load carriage and exosuit assistance. *Sci. Robot.* **7**, eabq1514 (2022).
19. Lee, U. H. et al. User preference optimization for control of ankle exoskeletons using sample efficient active learning. *Sci. Robot.* **8**, eadg3705 (2023).
20. Kim, J. et al. Reducing the energy cost of walking with low assistance levels through optimized hip flexion assistance from a soft exosuit. *Sci. Rep.* **12**, 11004 (2022).
21. Luo, S. et al. Experiment-free exoskeleton assistance via learning in simulation. *Nature* **630**, 353–359 (2024).
22. Molinaro, D. D. et al. Task-agnostic exoskeleton control via biological joint moment estimation, easier to deploy in terms of both actuation and computation. *Nature* **635**, 337–344 (2024).
23. Divekar, N. V., Thomas, G. C., Yerva, A. R., Frame, H. B. & Gregg, R. D. A versatile knee exoskeleton mitigates quadriceps fatigue in lifting, lowering, and carrying tasks. *Sci. Robot.* **9**, eadr8282 (2024).
24. Norris, J. A., Granata, K. P., Mitros, M. R., Byrne, E. M. & Marsh, A. P. Effect of augmented plantarflexion power on preferred walking speed and economy in young and older adults. *Gait Posture* **25**, 620–627 (2007).
25. Quinlivan, B. T. et al. Assistance magnitude versus metabolic cost reductions for a tethered multiarticular soft exosuit. *Sci. Robot.* **2**, eaah4416 (2017).
26. Poggensee, K. L. & Collins, S. H. How adaptation, training, and customization contribute to benefits from exoskeleton assistance. *Sci. Robot.* **6**, eabf1078 (2021).
27. Ingraham, K. A., Remy, C. D. & Rouse, E. J. The role of user preference in the customized control of robotic exoskeletons. *Sci. Robot.* **7**, eabj3487 (2022).
28. Beck, O. N. et al. Exoskeletons need to react faster than physiological responses to improve standing balance. *Sci. Robot.* **8**, eadf1080 (2023).
29. Slade, P. et al. On human-in-the-loop optimization of human-robot interaction. *Nature* **633**, 779–788 (2024).
30. Molinaro, D. D., Kang, I. & Young, A. J. Estimating human joint moments unifies exoskeleton control, reducing user effort. *Sci. Robot.* **9**, eadi8852 (2024).
31. Felt, W., Selinger, J. C., Donelan, J. M. & Remy, C. D. "body-in-the-loop": optimizing device parameters using measures of instantaneous energetic cost. *PloS ONE* **10**, e0135342 (2015).
32. Wen, Y., Si, J., Brandt, A., Gao, X. & Huang, H. H. Online reinforcement learning control for the personalization of a robotic knee prosthesis. *IEEE Trans. Cybern.* **50**, 2346–2356 (2019).
33. Ishmael, M. K., Archangeli, D. & Lenzi, T. Powered hip exoskeleton improves walking economy in individuals with above-knee amputation. *Nat. Med.* **27**, 1783–1788 (2021).
34. Han, H. et al. Selection of muscle-activity-based cost function in human-in-the-loop optimization of multi-gait ankle exoskeleton assistance. *IEEE Trans. Neural Syst. Rehabil. Eng.* **29**, 944–952 (2021).
35. Bryan, G. M. et al. Optimized hip–knee–ankle exoskeleton assistance at a range of walking speeds. *J. NeuroEng. Rehabil.* **18**, 1–12 (2021).
36. Gordon, D. F., McGreavy, C., Christou, A. & Vijayakumar, S. Human-in-the-loop optimization of exoskeleton assistance via online simulation of metabolic cost. *IEEE Trans. Robot.* **38**, 1410–1429 (2022).
37. Chen, Y. et al. Learning to assist different wearers in multitasks: efficient and individualized human-in-the-loop adaptation framework for lower-limb exoskeleton. *IEEE Trans. Robot.* **40**, 4699–4718 (2024).
38. Lakmazaheri, A. et al. Optimizing exoskeleton assistance to improve walking speed and energy economy for older adults. *J. NeuroEng. Rehabil.* **21**, 1 (2024).
39. Wang, W., Chen, J., Ding, J., Zhang, J. & Liu, J. Improving walking economy with an ankle exoskeleton prior to human-in-the-loop optimization. *Front. Neurorobotics* **15**, 797147 (2022).
40. Kantharaju, P. et al. Framework for personalizing wearable devices using real-time physiological measures. *IEEE Access* **11**, 81389–81400 (2023).
41. De Luca, C. J. The use of surface electromyography in biomechanics. *J. Appl. Biomech.* **13**, 135–163 (1997).
42. Grimmer, M., Zeiss, J., Weigand, F. & Zhao, G. Exploring surface electromyography (EMG) as a feedback variable for the human-in-the-loop optimization of lower limb wearable robotics. *Front. Neurorobotics* **16**, 948093 (2022).
43. Hansen, N., Müller, S. D. & Koumoutsakos, P. Reducing the time complexity of the derandomized evolution strategy with covariance matrix adaptation (cma-es). *Evol. Comput.* **11**, 1–18 (2003).
44. Sawicki, G. S. & Ferris, D. P. Mechanics and energetics of level walking with powered ankle exoskeletons. *J. Exp. Biol.* **211**, 1402–1413 (2008).
45. Shushtari, M., Foellmer, J. & Arami, A. Human–exoskeleton interaction portrait. *J. NeuroEng. Rehabil.* **21**, 152 (2024).
46. Ruder, S. An overview of gradient descent optimization algorithms. arXiv. https://doi.org/10.48550/arXiv.1609.04747 (2016).
47. Chen, J., Han, J. & Zhang, J. Design and evaluation of a mobile ankle exoskeleton with switchable actuation configurations. *IEEE/ASME Trans. Mechatron.* **27**, 1846–1853 (2022).
48. Witte, K. A., Zhang, J., Jackson, R. W. & Collins, S. H. Design of two lightweight, high-bandwidth torque-controlled ankle exoskeletons. In *Proc. 2015 IEEE International Conference on Robotics and Automation (ICRA)*, 1223–1228 (IEEE, 2015).
49. Zhang, J., Cheah, C. C. & Collins, S. H. Torque control in legged locomotion. In *Bioinspired Legged Locomotion*, 347–400 (Elsevier, 2017).
50. Chen, J., Ding, J., Han, J. & Zhang, J. Design and evaluation of a bilateral mobile ankle exoskeleton with high-efficiency actuation. *IEEE Robot. Autom. Lett.* **9**, 5528–5535 (2024).
51. Goldstein, D. S. Adrenal responses to stress. *Cell. Mol. Neurobiol.* **30**, 1433–1440 (2010).
52. Jacobsen, N. A. & Ferris, D. P. Electrocortical theta activity may reflect sensory prediction errors during adaptation to a gradual gait perturbation. *PeerJ* **12**, e17451 (2024).
53. Yin, W. et al. Stride-wise adaptive assistance strategy for ankle exoskeleton under varying walking conditions. *IEEE Trans. Neural Syst. Rehabil. Eng.* **33**, 3488–3497 (2025).
54. Liu, Z., Han, J., Han, J. & Zhang, J. Design and evaluation of a lightweight, ligaments-inspired knee exoskeleton for walking assistance. *IEEE Robot. Autom. Lett.* **9**, 8491 – 8498 (2024).
55. Wells, R. P. The projection of the ground reaction force as a predictor of internal joint moments. *Bull. Prosthet. Res.* **10**, 15–19 (1981).
56. Tan, X., Zhang, B., Liu, G., Zhao, X. & Zhao, Y. A time-independent control system for natural human gait assistance with a soft exoskeleton. *IEEE Trans. Robot.* **39**, 1653–1667 (2022).
57. Brockway, J. Derivation of formulae used to calculate energy expenditure in man. *Hum. Nutr. Clin. Nutr.* **41**, 463–471 (1987).

Acknowledgements

We thank Prof. Steven H. Collins from Stanford University for his suggestions on the design of studies. We thank Zhaoyuan Liu, Yingbo Song, and Qichong Bian for their help with video and photo shooting. We thank Zhibo Jing, Hexiang Yuan, and Qichong Bian for help with the experiments. This material was based on work supported by the National Natural Science Foundation of China under Grant 62073179, Beijing-Tianjin-Hebei Research Cooperation Project of China under Grant 24JCZXJC00340, and National Key Research and Development Programme of China under Grant 2022YFB4703003, all to Juanjuan Zhang.

Author contributions

Juanjuan Zhang, Jianyu Chen, and Jianda Han conceived the method; Juanjuan Zhang, Jianyu Chen and Lihai Zhang designed the studies; Juanjuan Zhang and Jianyu Chen implemented the experimental study platforms; Jianyu Chen, Weihao Yin, Jianquan Ding and Jiaqi Han conducted experimental studies; Juanjuan Zhang and Jianyu Chen analyzed data and prepared the supplementary data set; Juanjuan Zhang edited videos; Juanjuan Zhang and Jianyu Chen drafted the manuscript; all authors edited the manuscript and approved the submitted version.

Competing interests

Juanjuan Zhang, Jianyu Chen, and Jianda Han are inventors of the tethered unilateral and bilateral exoskeletons used in main and generality studies. Juanjuan Zhang and Jianyu Chen are inventors of the tethered knee exoskeleton and mobile exoskeleton control and actuation module. Other authors have no competing interests.

Additional information

Supplementary information The online version contains supplementary material available at https://doi.org/10.1038/s44172-025-00574-4.

Correspondence and requests for materials should be addressed to Juanjuan Zhang.

Peer review information *Communications Engineering* thanks Shuangyue Yu, Qifei Wu, Mohammad Shushtari and the other anonymous reviewer(s) for their contribution to the peer review of this work. Primary handling editors: [Philip Coatsworth]. A peer review file is available.